The Consultative Committee for Space Data Systems

Report Concerning Space Data System Standards

REAL-TIME WEATHER AND ATMOSPHERIC CHARACTERIZATION DATA

INFORMATIONAL REPORT

CCSDS 140.1-G-2

GREEN BOOK

March 2024

The Consultative Committee for Space Data Systems

Report Concerning Space Data System Standards

REAL-TIME WEATHER AND ATMOSPHERIC CHARACTERIZATION DATA

INFORMATIONAL REPORT

CCSDS 140.1-G-2

GREEN BOOK

March 2024

AUTHORITY

Issue:	Informational Report, Issue 2
Date:	March 2024
Location:	Washington, DC, USA

This document has been approved for publication by the Management Council of the Consultative Committee for Space Data Systems (CCSDS) and reflects the consensus of technical panel experts from CCSDS Member Agencies. The procedure for review and authorization of CCSDS Reports is detailed in *Organization and Processes for the Consultative Committee for Space Data Systems* (CCSDS A02.1-Y-4).

This document is published and maintained by:

CCSDS Secretariat
National Aeronautics and Space Administration
Washington, DC, USA
Email: secretariat@mailman.ccsds.org

FOREWORD

Through the process of normal evolution, it is expected that expansion, deletion, or modification of this document may occur. This Report is therefore subject to CCSDS document management and change control procedures, which are defined in *Organization and Processes for the Consultative Committee for Space Data Systems* (CCSDS A02.1-Y-4). Current versions of CCSDS documents are maintained at the CCSDS Web site:

http://www.ccsds.org/

Questions relating to the contents or status of this document should be sent to the CCSDS Secretariat at the email address indicated on page i.

At time of publication, the active Member and Observer Agencies of the CCSDS were:

Member Agencies

- Agenzia Spaziale Italiana (ASI)/Italy.
- Canadian Space Agency (CSA)/Canada.
- Centre National d'Etudes Spatiales (CNES)/France.
- China National Space Administration (CNSA)/People's Republic of China.
- Deutsches Zentrum für Luft- und Raumfahrt (DLR)/Germany.
- European Space Agency (ESA)/Europe.
- Federal Space Agency (FSA)/Russian Federation.
- Instituto Nacional de Pesquisas Espaciais (INPE)/Brazil.
- Japan Aerospace Exploration Agency (JAXA)/Japan.
- National Aeronautics and Space Administration (NASA)/USA.
- UK Space Agency/United Kingdom.

Observer Agencies

- Austrian Space Agency (ASA)/Austria.
- Belgian Science Policy Office (BELSPO)/Belgium.
- Central Research Institute of Machine Building (TsNIIMash)/Russian Federation.
- China Satellite Launch and Tracking Control General, Beijing Institute of Tracking and Telecommunications Technology (CLTC/BITTT)/China.
- Chinese Academy of Sciences (CAS)/China.
- China Academy of Space Technology (CAST)/China.
- Commonwealth Scientific and Industrial Research Organization (CSIRO)/Australia.
- Danish National Space Center (DNSC)/Denmark.
- Departamento de Ciência e Tecnologia Aeroespacial (DCTA)/Brazil.
- Electronics and Telecommunications Research Institute (ETRI)/Korea.
- Egyptian Space Agency (EgSA)/Egypt.
- European Organization for the Exploitation of Meteorological Satellites (EUMETSAT)/Europe.
- European Telecommunications Satellite Organization (EUTELSAT)/Europe.
- Geo-Informatics and Space Technology Development Agency (GISTDA)/Thailand.
- Hellenic National Space Committee (HNSC)/Greece.
- Hellenic Space Agency (HSA)/Greece.
- Indian Space Research Organization (ISRO)/India.
- Institute of Space Research (IKI)/Russian Federation.
- Korea Aerospace Research Institute (KARI)/Korea.
- Ministry of Communications (MOC)/Israel.
- Mohammed Bin Rashid Space Centre (MBRSC)/United Arab Emirates.
- National Institute of Information and Communications Technology (NICT)/Japan.
- National Oceanic and Atmospheric Administration (NOAA)/USA.
- National Space Agency of the Republic of Kazakhstan (NSARK)/Kazakhstan.
- National Space Organization (NSPO)/Chinese Taipei.
- Naval Center for Space Technology (NCST)/USA.
- Netherlands Space Office (NSO)/The Netherlands.
- Research Institute for Particle & Nuclear Physics (KFKI)/Hungary.
- Scientific and Technological Research Council of Turkey (TUBITAK)/Turkey.
- South African National Space Agency (SANSA)/Republic of South Africa.
- Space and Upper Atmosphere Research Commission (SUPARCO)/Pakistan.
- Swedish Space Corporation (SSC)/Sweden.
- Swiss Space Office (SSO)/Switzerland.
- United States Geological Survey (USGS)/USA.

DOCUMENT CONTROL

Document	Title	Date	Status
CCSDS 140.1-G-1	Real-Time Weather and Atmospheric Characterization Data, Informational Report, Issue 1	May 2017	Original issue, superseded
CCSDS 140.1-G-2	Real-Time Weather and Atmospheric Characterization Data, Informational Report, Issue 2	March 2024	Current issue

CONTENTS

CONTENTS (continued)

Figure Page

CONTENTS (continued)

1 INTRODUCTION

1.1 PURPOSE AND SCOPE

Space-to-ground optical communications are affected by the presence of cloud cover and other atmospheric effects. Therefore it is important to specify, accurately measure, analyze, characterize, and ultimately predict critical atmospheric parameters for the purposes of:

– selection of Optical Ground Stations (OGS);

– development of concepts of operation, including real-time knowledge of atmospheric parameters needed to make link handover decisions;

– evaluation of the long-term atmospheric characteristics of OGS; and

– development of link budgets.

The purpose of this Report is to identify and describe the atmospheric constituents that are most responsible for transmission losses in optical communications links at wavelengths near 1550 and 1064 nm. This book contains a full description of the critical atmospheric parameters and describes suggested types of instruments that can be used to measure these parameters. Although this book includes examples of existing instruments that have been deployed and are currently being used for optical communications applications, it does not provide any recommendations regarding particular instruments or instrument manufacturers. This book also describes examples of prediction systems that have been considered by space agencies and discusses the types of algorithms that may be necessary to enable these systems. Considerations concerning the temporal measurement of the atmospheric parameters are discussed, along with the possible ways the data can be used for long-term OGS characterization and real-time operations, including handover prediction support.

1.2 DOCUMENT STRUCTURE

This book consists of six main sections and two annexes. Section 1 contains introductory material. Section 2 discusses the motivation for atmospheric data collection and background information on the important atmospheric parameters. Section 3 lists and describes the physical quantities that must be measured or derived to determine the atmospheric parameters necessary to support OGS selection and operations of optical communications systems. Section 4 describes the types of instruments that are necessary for real-time and long-term collection of the physical quantities described in section 3 and provides examples of several instruments currently in use. Section 5 provides suggestions regarding the temporal collection of the atmospheric data. Section 6 discusses how the data can be used to analyze the long-term characteristics of OGS and to enable site selection, as well as how this data may be used to facilitate real-time decision making and site operations. Annex A describes several physical parameters that may be measured or derived, but are not considered critical for OGS selection or operations. Annex A also describes the instruments corresponding to the parameters that may be measured. Annex B lists abbreviations and acronyms contained in this document.

1.3 REFERENCES

The following publications are referenced in this document. At the time of publication, the editions indicated were valid. All publications are subject to revision, and users of this document are encouraged to investigate the possibility of applying the most recent editions of the publications indicated below. The CCSDS Secretariat maintains a register of currently valid CCSDS publications.

[1] Randall J. Alliss and Billy Felton. "Realtime Atmospheric Decision Aids in Support of the Lunar Laser Communications Demonstration." In *Proceedings of the 2014 International Conference on Space Optical Systems and Applications (ICSOS) (7–9 May 2014, Kobe, Japan)*. Tokyo: NICT, 2014.

[2] *Optical Link Study Group Addendum to Final Report*. IOAG.T.OLSG.2012.V1A. Washington, DC: IOAG, November 2012.

[3] *Optical Link Study Group Final Report*. IOAG.T.OLSG.2012.V1A. Washington, DC: IOAG, June 2012.

[4] Kenji Suzuki, et al. "Environmental Data Gathering System for Satellite-to-Ground Station Optical Communications." In *Proceedings of the 2014 International Conference on Space Optical Systems and Applications (ICSOS) (7–9 May 2014, Kobe, Japan)*. Tokyo: NICT, 2014.

[5] *Propagation Data Required for the Design of Earth-Space Systems Operating between 20 THz and 375 THz*. ITU-R P.1621-2. Geneva: ITU, 2015.

[6] *ATST Site Survey Working Group Final Report*. Revision A. Report #0021. Tucson, Arizona: NSO, October 6, 2004.

[7] Lianqi Wang, et al. "High Accuracy DIMM Measurements for the TMT Site Testing Program." In *Ground-Based and Airborne Telescopes*. Edited by Larry M. Stepp. Proceedings of SPIE Vol. 6267. Bellingham, Washington: SPIE, 15 June 2006.

[8] Randall J. Alliss and Billy D. Felton. "Numerical Simulations of Optical Turbulence Using an Advanced Atmospheric Prediction Model: Implications for Adaptive Optics Design." In *Proceedings of the Advanced Maui Optical and Space Surveillance Technologies Conference (9–12 September 2014, Maui, Hawaii)*. Edited by S. Ryan. Maui, Hawaii: AMOS, 2014.

[9] B. N. Holben, et al. "AERONET—A Federated Instrument Network and Data Archive for Aerosol." *Remote Sensing of Environment* 66, no. 1 (October 1998): 1–16.

[10] *Attenuation Due to Clouds and Fog*. ITU-R P.840-6. Geneva: ITU, 2013..

[11] Joseph A. Shaw, et al. “Cloud Optical Depth Measured with Ground-Based, Uncooled Infrared Imagers.” In *Remote Sensing of the Atmosphere, Clouds, and Precipitation IV*. Edited by Tadahiro Hayasaka, Kenji Nakamura, and Eastwood Im. Proceedings of SPIE Vol. 8523. Bellingham, Washington: SPIE, 27 November 2012.

[12] D. L. Fried. “Optical Resolution through a Randomly Inhomogeneous Medium for Very Long and Very Short Exposures.” *Journal of the Optical Society of America* 56, no. 10 (1 October 1966): 1372–1379.

[13] J. L. Mohr, R. A. Johnston, and P. L. Cottrell. “Optical Turbulence Measurements and Models for Mount John University Observatory.” *Publications of the Astronomical Society of Australia* 27, no. 3 (2010): 347–359.

[14] M. Sarazin and F. Roddier. “The ESO Differential Image Motion Monitor.” *Astronomy and Astrophysics* 227, no. 1 (January 1990): 294–300.

[15] Jingquan Cheng. *The Principles of Astronomical Telescope Design*. Astrophysics and Space Science Library 360. New York: Springer, 2009.

[16] Larry C. Andrews and Ronald L. Phillips. *Laser Beam Propagation through Random Media*. 2nd ed. Bellingham, Washington: SPIE, 2005.

[17] G. C. Loos and C. B. Hogge. “Turbulence of the Upper Atmosphere and Isoplanatism.” *Applied Optics* 18, no. 15 (1 August 1979): 2654–2661.

[18] M. Sarazin and A. Tokovinin. “The Statistics of Isoplanatic Angle and Adaptive Optics Time Constant Derived from DIMM Data.” In *Beyond Conventional Adaptive Optics: A Conference Devoted to the Development of Adaptive Optics for Extremely Large Telescopes—Proceedings of the Topical Meeting Held May 7–10, 2001, Venice, Italy*. Edited by E. Vernet, et al. ESO Conference and Workshop Proceedings 58. Garching, Germany: European Southern Observatory, 2002.

[19] Alexander Berk, Lawrence S. Bernstein, and David C. Robertson. *MODTRAN: A Moderate Resolution Code for LOWTRAN 7*. GL-TR-89-C122. Hanscom Air Force Base, Massachusetts: United States Air Force, 1989.

[20] Sabino Piazzolla, et al. “Preliminary Assessement of the Atmospheric Optical Channel at Goldstone (CA).” In *Proceedings of the 2011 International Conference on Space Optical Systems and Applications (ICSOS) (11–13 May 2011)*, 220–227. Piscataway, New Jersey: IEEE Conference Publications, 2011.

[21] Kevin Shortt, et al. “Implications of Sky Radiance on Deep Space Optical Communication Links.” In *Proceedings of the 65th International Astronautical Congress (29 September–3 October 2014, Toronto, Canada)*. Paris, France: International Astronautical Federation, 2014.

[22] F. I. Khatri and A. Biswas. "Signal and Background Levels for the Mars Laser Communications Demonstration (MLCD)." In *Digest of the LEOS Summer Topical Meetings (25–27 July 2005)*, 25–26. Piscataway, New Jersey: IEEE Conference Publications, 2005.

[23] A. Biswas and S. Piazzolla. "The Atmospheric Channel." Chapter 3 in *Deep Space Optical Communications*. Edited by Hamid Hemmati. JPL Deep Space Communications and Navigation Series. Hoboken, New Jersey: Wiley, April 2006.

[24] A. Biswas and S. Piazzolla. "Deep-Space Optical Communications Downlink Budget from Mars: System Parameters." *The Interplanetary Network Progress Report* 42, no. 154 (August 2003): 1–38.

[25] Dimitri Klebe, et al. "All-Sky Mid-Infrared Imagery to Characterize Sky Conditions and Improve Astronomical Observational Performance." *Publications of the Astronomical Society of the Pacific* 124, no. 922 (20 November 2012): 1309–1317.

[26] Paul W. Nugent, Joseph A. Shaw, and Sabino Piazzolla. "Infrared Cloud Imaging in Support of Earth-Space Optical Communication." *Optics Express* 17, no. 10 (2009): 7862–7872.

[27] Paul W. Nugent, et al. "Correcting Calibrated Infrared Sky Imagery for the Effect of an Infrared Window." *Journal of Atmospheric and Oceanic Technology* 26, no. 11 (November 2009): 2403–2412.

[28] Paul W. Nugent, Joseph A. Shaw, and Sabino Piazzolla. "Infrared Cloud Imager Development for Atmospheric Optical Communication Characterization, and Measurements at the JPL Table Mountain Facility." *The Interplanetary Network Progress Report* 42, no. 192 (February 15, 2013).

[29] "Title 21: Food and Drugs: Part 1040—Performance Standards for Light-Emitting Products: §1040.10 Laser Products." Electronic Code of Federal Regulations. http://www.ecfr.gov/cgi-bin/text-idx?node=se21.8.1040_110&rgn=div8.

[30] "Title 21: Food and Drugs: Part 1040—Performance Standards for Light-Emitting Products: §1040.11 Specific Purpose Laser Products." Electronic Code of Federal Regulations. http://www.ecfr.gov/cgi-bin/text-idx?node=se21.8.1040_111&rgn=div8.

[31] A. Tokovinin. "From Differential Image Motion to Seeing." *Publications of the Astronomical Society of the Pacific* 114, no. 800 (October 2002): 1156-1166.

[32] S. A. Ehgamberdiev, et al. "The Astroclimate of Maidanak Observatory in Uzbekistan." *Astronomy and Astrophysics Supplement Series* 145, no. 2 (August 2000): 293–304.

[33] Jacques M. Beckers. "A Seeing Monitor for Solar and Other Extended." *Experimental Astronomy* 12, no. 1 (August 2001): 1–20.

[34] H. Socas-Navarro, et al. “Solar Site Survey for the Advanced Technology Solar Telescope. I. Analysis of the Seeing Data.” *Publications of the Astronomical Society of the Pacific* 117 (November 2005): 1296–1305.

[35] Glenn E. Shaw. “Sun Photometry.” *Bulletin of the American Meteorological Society* 64, no. 1 (January 1983): 4–10.

[36] Toyoshima Morio, et al. “Overview of the Laser Communication System for the NICT Optical Ground Station and Laser Communication Experiments on Ground-to-Satellite Links.” *Journal of the National Institute of Information and Communications Technology* 59, no. 1–2 (March–June 2012): 53–75.

[37] Gary S. Wojcik, et al. “Deep-Space to Ground Laser Communications in a Cloudy World.” In *Free-Space Laser Communications (July 31, 2005, San Diego, California)*. Edited by David G. Voelz and Jennifer C. Ricklin. Proceedings of SPIE Vol. 5892. Bellingham, Washington: SPIE, 2005.

[38] W. Paul Menzel and James F. W. Purdom. “Introducing GOES-I: The First of a New Generation of Geostationary Operational Environmental Satellites.” *Bulletin of the American Meteorological Society* 75, no. 5 (May 1994): 757–781.

[39] C. G. Hanson, et al. “Meteosat Second Generation: Seviri Radiometric Performance Results from the MSG-1 Commissioning Phase.” http://citeseerx.ist.psu.edu/viewdoc/download?doi=10.1.1.10.5241&rep=rep1&type=pdf.

[40] Jeffery J. Puschell, et al. “Japanese Advanced Meteorological Imager: A Next Generation GEO Imager for MTSAT-1R.” In *Earth Observing Systems VII (September 25, 2002)*, 152–161. Edited by William L. Barnes. Proceedings of SPIE Vol. 4814. Bellingham, Washington: SPIE, 2002.

[41] Donald L. Walters and L. William Bradford. “Measurements of r_0 and θ_0: Two Decades and 18 Sites.” *Applied Optics* 36, no. 30 (1997): 7876-7886.

[42] Billy D. Felton, Philip D. Hayes, and Randall J. Alliss. “Improved Atmospheric Characterization for Free-Space Link Analysis Using Numerical Weather Prediction.” In *Atmospheric Propagation IX*. Edited by Linda M. Wasiczko Thomas and Earl J. Spillar. Proceedings of SPIE Vol. 8380. Bellingham, Washington: SPIE, 5 May 2012.

[43] Randall J. Alliss, Billy D. Felton, and Eric M. Kemp. “Simulations of Optical Turbulence via Numerical Weather Prediction for Use in Optical Communication Studies.” In *Proceedings of the Advanced Maui Optical and Space Surveillance Technologies Conference (17–19 September 2008, Maui, Hawaii)*. Edited by S. Ryan. Maui, Hawaii: AMOS, 2008.

[44] Randall J. Alliss, et al. “Atmospheric Cloud Forecasting in Support of Space Based Applications.” In *Proceedings of the Advanced Maui Optical and Space Surveillance Technologies Conference (10–13 September 2013, Maui, Hawaii)*. Edited by S. Ryan. Maui, Hawaii: AMOS, 2013.

[45] M. Steven Tracton and Jun Du. “Short Range Ensemble Forecasting (SREF) at NCEP/EMC.” In *Proceedings of the Sixth Workshop on Meteorological Operational Systems (17–21 November 1997, Reading, United Kingdom)*. Reading, United Kingdom: ECMWF, 1998.

[46] Barry A. Bodhaine, et al. “On Rayleigh Optical Depth Calculations.” *Journal of Atmospheric and Oceanic Technology* 16, no. 11 (November 1999): 1854–1861.

[47] G. P. Anderson, et al. “FASCODE/MODTRAN/LOWTRAN: Past/Present/Future.” In *Proceedings of the 18th Annual Review Conference on Atmospheric Transmission Models (6–8 June 1995, Bedford, Massachusetts)*, 101–143. Edited by Gail P. Anderson, Richard H. Picard, and James H. Chetwynd. Hanscom Air Force Base, Massachusetts: Phillips Laboratory, 18 April 1996.

[48] H. J. P. Smith, et al. *FASCODE—Fast Atmospheric Signature Code (Spectral Transmittance and Radiance)*. AFGL-TR-78-0081. Burlington, Massachusetts: Visidyne, Inc., 16 January 1978.

[49] L. S. Rothman, et al. “The HITRAN2012 Molecular Spectroscopic Database.” *Journal of Quantitative Spectroscopy and Radiative Transfer* 130 (November 2013): 4–50.

[50] Jinxue Wang, et al. “Validation of FASCOD3 and MODTRAN3: Comparison of Model Calculations with Ground-Based and Airborne Interferometer Observations under Clear-Sky Conditions.” *Applied Optics* 35, no. 30 (1996): 6028–6040.

[51] H. T. Yura and W. G. McKinley. “Aperture Averaging of Scintillation for Space-to-Ground Optical Communication Applications.” *Applied Optics* 22, no. 11 (1983): 1608–1609.

[52] Abhijit Biswas, et al. “Uplink Beacon Laser for Mars Laser Communication Demonstration (MLCD).” In *Free-Space Laser Communication Technologies XVII*, 93–100. Edited by G. Stephen Mecherle. Proceedings of SPIE Vol. 5712. Bellingham, Washington: SPIE, 2005.

[53] W. M. Hughes and R. B. Holmes. “Pupil-Plane Imager for Scintillometry over Long Horizontal Paths.” *Applied Optics* 46, no. 29 (2007): 7099–7109.

[54] N. Perlot, et al. “Results of the Optical Downlink Experiment KIODO from OICETS Satellite to Optical Ground Station Oberpfaffenhofen (OGS-OP).” In *Free-Space Laser Communication Technologies XIX and Atmospheric Propagation of Electromagnetic Waves*. Edited by Steve Mecherle and Olga Korotkova. Proceedings of SPIE Vol. 6457. Bellingham, Washington: SPIE, February 2007.

[55] Joachim Horwath, et al. "Experimental Verification of Optical Backhaul Links for High-Altitude Platform Networks: Atmospheric Turbulence And Downlink Availability." *International Journal of Satellite Communications and Networking* 25, no. 5 (501–528).

[56] Michael G. Dittman. "Contamination Scatter Functions for Stray-Light Analysis." In *Optical System Contamination: Effects, Measurements, and Control VII*. Edited by Philip T. C. Chen and O. Manuel Uy. Proceedings of SPIE Vol. 4774. Bellingham, Washington: SPIE, September 2002.

[57] Randall J. Alliss. "Optimizing the Performance of Space to Ground Optical Communications." In *Proceedings of Free-Space Laser Communications XXXI (4–6 February 2019, San Francisco)*. Edited by Hamid Hemmati and Don M. Boroson. Proceedings Volume 10910. Bellingham, Washington: SPIE, 2019.

[58] Randall J. Alliss. "A Novel Approach for Simulating Atmospheric Optical Turbulence Seeing Parameters." In *Proceedings of the Advanced Maui Optical and Space Surveillance Technologies Conference (AMOS) 2023 (19–22 September 2023, Maui, Hawaii)*. Kihei, Hawaii: Maui Economic Development Board, 2023.

[59] M.E. Craddock, R.J. Alliss, and M. Mason. "Improving the Accuracy of Cloud Detection Using Machine Learning." Presented at The American Geophysical Union (AGU) Fall Meeting 2017 (11–15 December 2017, New Orleans).

[60] Danny Felton, et al. "Accelerated AI Powered Atmospheric Predictions for Space Domain Awareness Applications." In *Proceedings of the Advanced Maui Optical and Space Surveillance Technologies Conference (AMOS) 2021 (14–17 September 2021, Maui, Hawaii)*. Kihei, Hawaii: Maui Economic Development Board, 2021.

[61] Mary Ellen Craddock, et al. "Validation of Atmospheric Characterization and Prediction over Haleakala during the Laser Communications Relay Demonstration." In *Proceedings of the Advanced Maui Optical and Space Surveillance Technologies Conference (AMOS) 2022 (27–30 September 2022, Maui, Hawaii)*. Kihei, Hawaii: Maui Economic Development Board, 2022.

[62] Alexandria M. Russell, Randall J. Alliss, and Billy D. Felton. "A Deep Machine Learning Algorithm to Optimize the Forecast of Atmospherics." In *Proceedings of the Advanced Maui Optical and Space Surveillance Technologies Conference (AMOS) 2017 (19–22 September 2017, Maui, Hawaii)*. Kihei, Hawaii: Maui Economic Development Board, 2017.

[63] Randall J. Alliss. "Atmospheric Characterization of the Space Environment: Unique Observations from Haleakala." In *Proceedings of the Advanced Maui Optical and Space Surveillance Technologies Conference (AMOS) 2019 (17–20 September 2019, Maui, Hawaii)*. Kihei, Hawaii: Maui Economic Development Board, 2019.

[64] Dimitar R. Kolev, et al. “Cloud Statistics for NICT Optical Ground Station Sites Using Environmental-Data Collection System Experimental Data.” Presented at Satellite Communication Session. Lecture Number B-3-20. https://www.ieice.org/publications/search/summary.php?id=CONF0000115992&tbl=conf&lang=en

[65] Mary Ellen Craddock, et al. “The Lasercom Atmospheric Monitoring and Prediction System.” In *Proceedings of Free-Space Laser Communications XXXVI (30–31 January 2024, San Francisco)*. Proceedings Volume 12413, Free-Space Laser Communications XXXV. Bellingham, Washington: SPIE, forthcoming.

[66] Kenji Suzuki, et al. “Environmental Data Gathering System for Satellite-to-Ground Station Optical Communications.” In *Proceedings of the International Conference on Space Optical Systems and Applications (ICSOS) 2014 (7–9 May 2014, Kobe, Japan)*. Tokyo: NICT, 2014.

[67] Kenji Suzuki, et al. “Environmental-Data Collection System for Satellite-to-Ground Optical Communications.” *Trans. JSASS Aerospace Tech. Japan* 16, no. 1 (2018): 35–39.

[68] K. Saucke, et al. “Characterisation of the Optical Channel GEO to Ground: Using Five Years of Data from Alphasat TDP1 and T-AOGS for Investigation of Different Conditions.” In *Proceedings of International Conference on Space Optics—ICSO 2021 (30 March–2 April 2021, Online Only)*. Proceedings Volume 11852, International Conference on Space Optics—ICSO 2020. Bellingham, Washington: SPIE, 2021.

2 OVERVIEW

2.1 MOTIVATION

Space-to-ground optical communications have tremendous potential to help meet future data volume demands. However, free-space optical signals are adversely affected by the presence of cloud cover and optical turbulence and, to a lesser extent, by aerosols in the atmosphere. These atmospheric challenges to operational optical communications systems are illustrated in figure 2-1, which shows Geostationary (GEO) and Low Earth Orbiting (LEO) satellites interacting with and working around atmospheric degradations. Each of these atmospheric effects may require one or more different mitigation strategies, which may in turn be dependent on the operational design of a particular system.

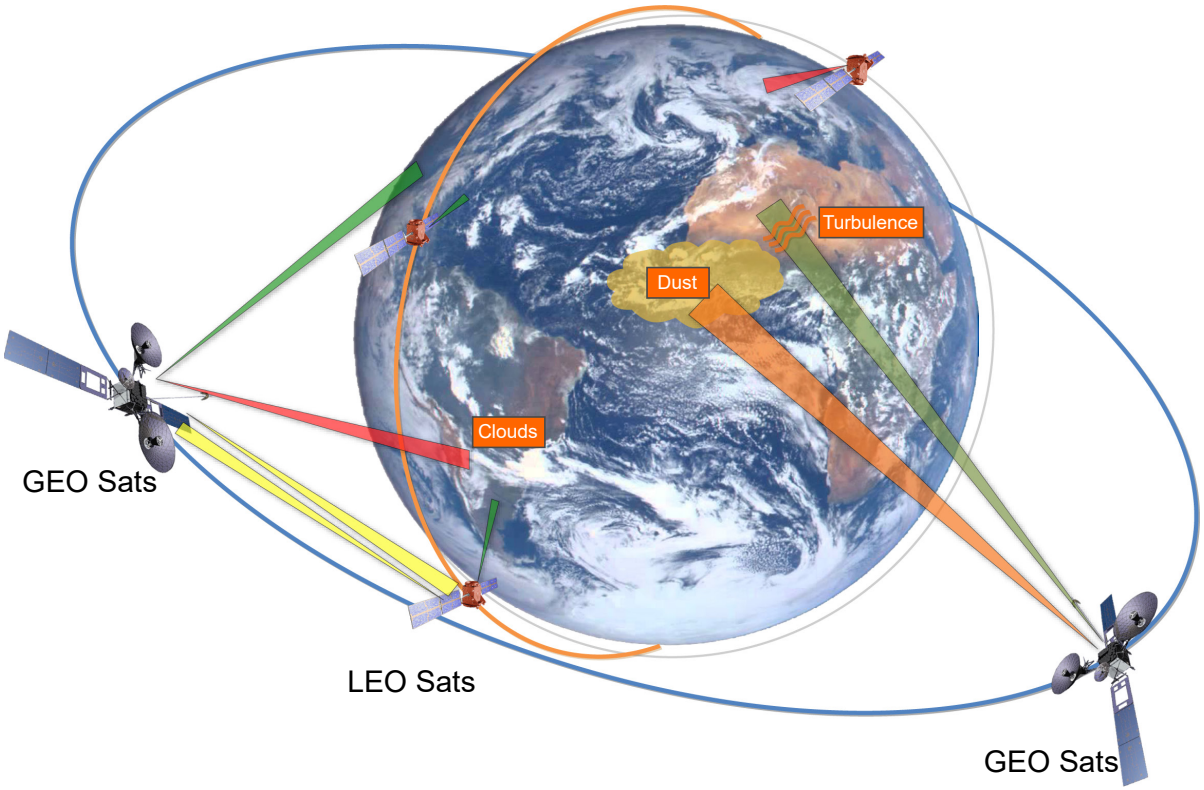

Figure 2-1: Conceptual Illustration of Atmospheric Effects Experienced by Space-to-Ground Optical Communications

In figure 2-1, GEO and LEO satellites are shown orbiting the Earth. Optical links are shown by the cones: dark green represents a Cloud Free Line of Sight (CFLOS) and thus full data rate link, light green represents a link degraded by turbulence, orange represents a link attenuated by aerosols, red represents a link blocked by clouds, and yellow indicates an uplink from a LEO to a GEO.

Clouds are the largest source of atmospheric attenuation for space-to-ground optical signals. Although it is possible to successfully communicate through some clouds, it is not practical to include sufficient margin in the link budget to completely prevent cloud blockages. In the example shown in figure 2-1, the negative impact of clouds on the optical links from the GEO satellites is reduced by 'ground station diversity'. In this concept, multiple stations have the potential to receive communications when other sites are cloud covered or unavailable because of geometric visibility limitations. This mitigation strategy is effective since weather systems have limited extents, and clouds are affected by solar radiation, terrain, and other variable parameters. Therefore combinations of ground sites can be identified to improve the cloud-free availability of optical communications systems. The number and spacing of the ground stations will be highly dependent on a particular system's concept of operations. Clouds will also affect LEO operations. However, LEO satellites will generally not be able to see multiple, widely spaced ground stations simultaneously. As such, LEO satellites may be required to use an alternative mitigation strategy, such as storing data on board or transmitting data to GEO satellites to minimize data loss caused by cloud interruptions. The effective mitigation of communication outages due to clouds is improved by knowing the long-term cloud statistics and by characterizing and forecasting clouds in real time to support link handovers.

Although clouds are the primary source of optical signal attenuation, Optical Turbulence (OT) also degrades optical transmissions. OT distorts light as it travels through the atmosphere. It creates fluctuations in the power received by the ground station and causes distortions of the phase of the transmitted wave. This effect is illustrated in the left panel of figure 2-2, in which the intensity of the signal is seen to be irregular upon the receiver's focal plane. There are several strategies to reduce or compensate for the effects of OT. One method is to use Adaptive Optics (AO) to correct phase distortions. The impact of this method is demonstrated in the right panel of figure 2-2, in which the signal has been corrected using AO. The severity of OT, and thus the amount of correction required, is largely dependent upon the local turbulence at the site.

To support correction for OT, accurate characterization of the long-term OT statistics at OGS is recommended. For example, long-term collection of OT can assist engineers in developing optimal coding and modulation techniques. In addition, real-time collection of OT is recommended to describe the performance of the link and to diagnose transmission errors.

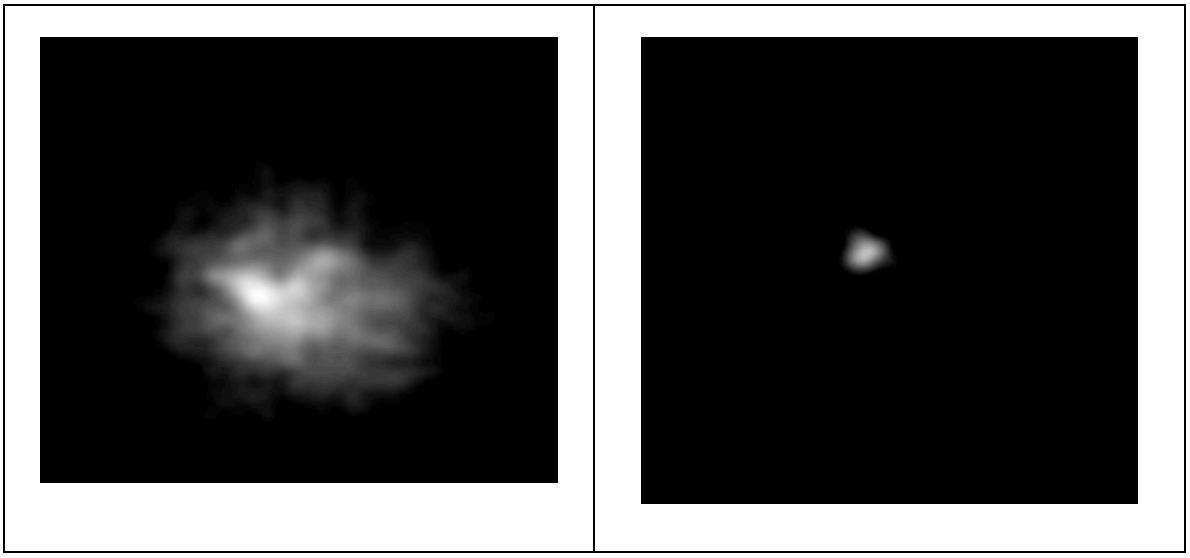

Figure 2-2: Turbulence and Adaptive Optics

Although the effect of aerosol concentration is not a primary attenuating parameter (fade is typically less than 1 dB) for optical communications, it is still important to characterize aerosols at OGS and account for aerosols in the system's link budget. Composed of particles and droplets suspended in the atmosphere, the aerosol loading in the atmosphere can vary significantly according to location and time of year. For example, an optical ground station located on Tenerife would experience large transmission losses due to the Calima (Saharan dust) events that occur periodically in the spring and summer months.

Operations of optical communications systems may also be affected by meteorological conditions. For example, the ground station may need to be closed during high wind conditions to protect the physical structures. Precipitation or condensation may force closure of a dome to protect sensitive optical equipment.

Subsection 2.2 provides additional background information on the primary atmospheric parameters affecting optical communications: clouds, optical turbulence, aerosols, and standard meteorological quantities.

2.2 BACKGROUND ON PRIMARY ATMOSPHERIC PARAMETERS

2.2.1 INTRODUCTION

The subsections below discuss details regarding the critical atmospheric parameters affecting optical communications links. Other sections in the document contain additional information about these parameters: section 3 discusses the physical quantities that need to be measured to characterize these atmospheric parameters, section 4 discusses the types of instruments used to measure those physical quantities, section 5 discusses recommendations regarding the temporal collection of the atmospheric data, and section 6 discusses how the data can be used for both long-term site characterization and real-time decision making.

2.2.2 CLOUDS

Clouds pose a serious attenuation problem for space-to-Earth communications at optical wavelengths. Clouds are composed of water droplets and/or ice crystals that scatter and absorb optical wavelengths. They occur on scales that range from less than a single kilometer to thousands of kilometers. As such, they not only cause problems for links to individual ground stations but can also simultaneously attenuate optical signals at multiple ground stations given their large geographical extent. This subsection provides some background on how clouds have been measured and characterized, and how the resulting data has been used in the recent past to support optical communications applications.

Atmospheric transmission losses exceeding several decibels are frequent in most clouds, even cirrus clouds. Figure 2-3 shows how cloud liquid water content, cloud thickness, and the elevation angle of an optical link affect the transmission loss through typical clouds: thin cirrus (top left), thicker cirrus (top right), stratus cloud (bottom left), and cumulus cloud (bottom right). Clouds composed primarily of water droplets, such as stratus and cumulus, can be considered obstacles to optical communications because of the high attenuation they impose on an optical link (bottom panels of figure 2-3). Cirrus clouds, comprised largely of ice crystals, generally have a smaller impact on optical signals than do water clouds. However, even in cirrus clouds, transmission losses often exceed 3 dB, with the exact losses depending on the vertical extent of the cloud and its temperature. Additionally, ‘thin’ cirrus clouds are not homogeneous, but contain optically thick portions that can cause large fluctuations in signal strength on time scales of less than one minute.

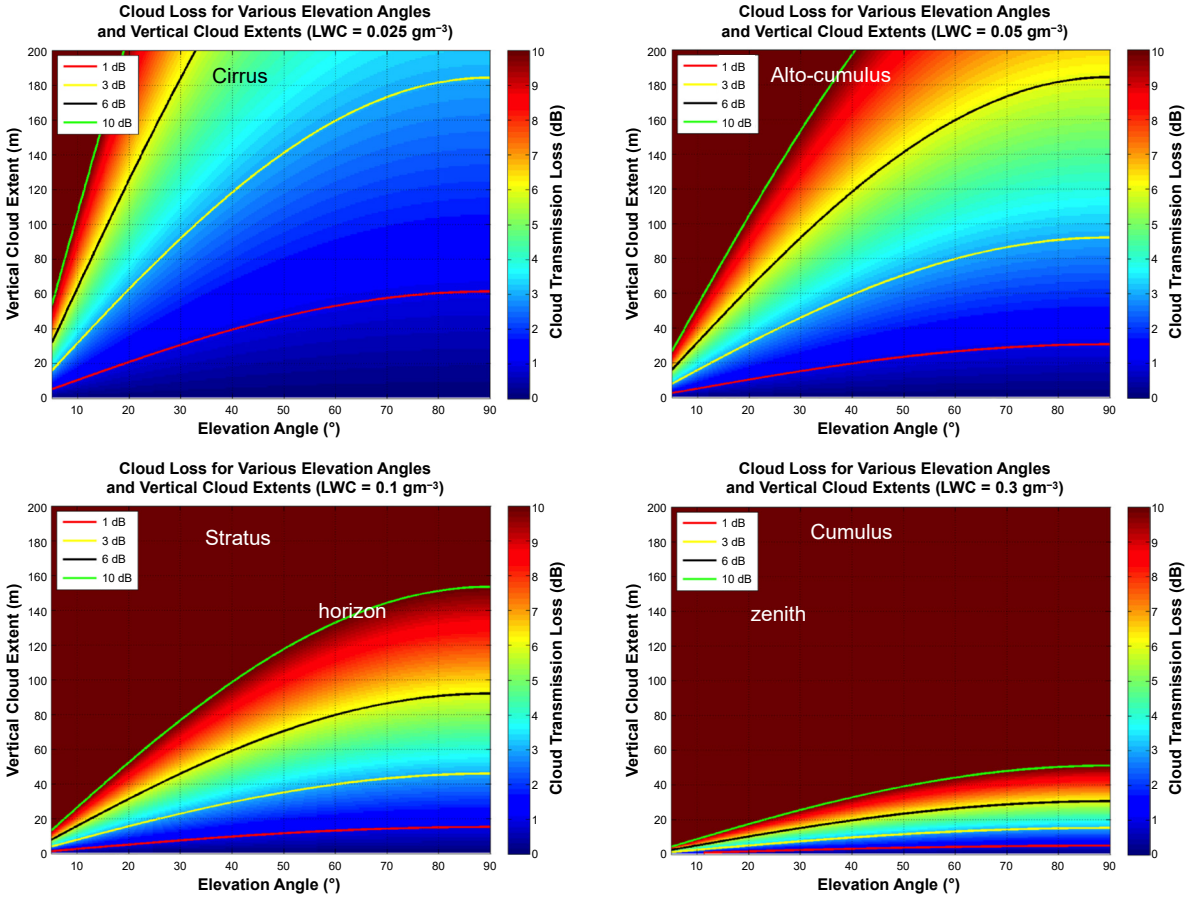

Figure 2-3: Cloud Transmission Loss

NOTE – Figure 2-3 shows cloud transmission loss due to typical thin (top left) and thicker (top right) cirrus clouds, stratus clouds (bottom left), and cumulus clouds (bottom right) as a function of elevation angle and physical thickness of the cloud for specific values of Liquid Water Content (LWC). Fade increases with increasing cloud thickness and decreasing elevation angle (see reference [1]).

Given the significant impacts of most clouds on optical communications signals, a mitigation strategy is needed to maximize the transfer of data and the overall availability of the optical communications system. As discussed earlier, one effective cloud mitigation strategy involves using ground station diversity to increase the probability that a CFLOS exists from a spacecraft to at least one ground site at any given time. Typical meteorological patterns cause the cloud cover at stations within a few hundred kilometers of each other to be correlated because cloud systems generally occur on scales of many hundreds of kilometers. Given this knowledge and an accurate characterization of long-term cloud statistics at multiple locations, a network of multiple ground sites can be created to maximize system availability.

For example, a site optimization study conducted for a satellite in an L1 orbit (see reference [2]) shows the effects of site diversity. In this example, the spacecraft is always attempting to send data to the ground, so the stations not only need to be geographically diverse, but also close enough to each other to maintain continuous visibility to the spacecraft as its position with respect to the Earth's surface changes with time. This situation may not be a requirement in all concepts of operations, but was assumed for the purposes of this particular study. The resulting network of 10 ground stations is shown in figure 2-4. Given the geometry of the L1 orbit, the spacecraft only has visibility to 3–4 ground stations at any given time yet still provides a cloud-free availability of approximately 95 percent. The average station spacing in this example is on the order of 10^3 km partly because of the L1 orbit and partly because of the desire to minimize the effects of correlated atmospherics. The highest availability of any one ground station in this network is about 32 percent, taking into account satellite visibility and CFLOS.

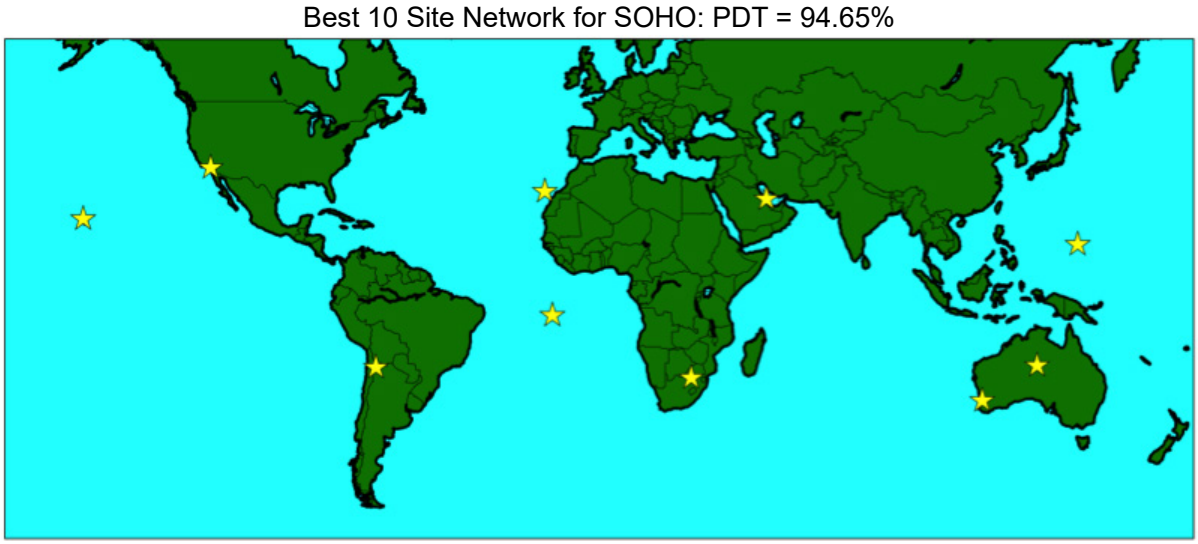

Figure 2-4: Geographically Diverse Ground Network

Figure 2-4 is a depiction of a geographically diverse network of ground sites for an L1 Space-to-Ground concept of operations. Percent Data Transferred (PDT) is 94.65 percent (see reference [2]). PDT in this example is an example of link availability, which includes the impact of clouds and geometry.

This study could not have been performed without a long-term, high-fidelity, global database of clouds. In fact, over the last several years, a significant amount of work has been performed to characterize clouds in support of Free-Space Optical Communications (FSOC) (see references [2], [3], and [57]). Years of multispectral imagery have been gathered remotely by satellites, and the raw data have been converted to cloud decision products to provide a powerful foundation for future system optimization studies. The long-term, global cloud data is vital to site selection studies, assisting system designers not only to determine the optimal site or group of sites to meet mission objectives, but to estimate the expected performance of a system. Field campaigns have also been conducted by a number of groups to characterize individual locations at higher spatial and temporal resolutions than can be provided by satellites (see reference [4]).

Going forward, system designers may wish to supplement the satellite-based cloud database with high-resolution ground-based measurements of clouds. Long-term in-situ measurements can be used to validate the satellite studies. Additionally, once an optical communications system becomes operational, real-time characterization of clouds can be used to inform intelligent link handover decisions. The cloud data can be used to identify sites that are currently cloudy or cloud-free, predict near-term cloud attenuation and outages, and identify the best site to which to transfer the link.

2.2.3 OPTICAL TURBULENCE (ATMOSPHERIC SEEING PARAMETERS)

Optical turbulence is a significant challenge to high-data-rate space-to-Earth and Earth-to-space optical communications. Small-scale variations in the density of the atmosphere create inhomogeneities in its refractive index and produce distortions in the radiation wavefront. This distortion causes fluctuations in the amplitude and phase of electromagnetic waves propagating through the atmosphere, degrading optical signal quality. The overall degradation in signal quality resulting from these random phase aberrations is often defined as 'astronomical seeing' but is referred to in this Report as 'atmospheric seeing'. The strength of the fluctuations of the atmospheric refractive index is quantified by the refractive index structure parameter, C_n^2 [$m^{2/3}$]. Knowledge of the C_n^2 profile in the atmosphere can be used to derive several standard atmospheric seeing parameters, including the atmospheric coherence length (Fried parameter), the isoplanatic angle (see reference [5]), as well as the scintillation index, σ_I^2. Because it is impractical to accurately measure C_n^2 along a path from an OGS to a satellite, instruments will be deployed to quantify the Fried parameter and isoplanatic angle. The main body of this document describes only the minimum set of parameters that are vital for OGS characterization and that require a dedicated instrument for their measurement. Other parameters that are not used in OGS selection, such as the scintillation index, σ_I^2, can be derived directly from the operational system and are therefore described in annex A.

The ability to characterize the OT at ground station locations is vital to the mitigation of its effects on the optical communications link. For example, when site selection investigations for large telescopes are performed, extensive campaigns are conducted to monitor and quantify the atmospheric seeing conditions at candidate sites. These investigations are generally conducted using atmospheric seeing monitors such as a Differential Image Motion Monitor (DIMM) to detect the range of turbulence conditions that occur at those sites. For example, OT characterization was performed for the Daniel K. Inouye Solar Telescope (see reference [6]), which is to be built on the summit of Haleakala in Hawaii, and the Thirty Meter Telescope (TMT), which is under construction on Mauna Kea in Hawaii (see reference [7]).

A precursor to in-situ measurements is to use numerical simulations of OT to provide an estimate of atmospheric seeing conditions in regions where infrastructure (e.g., electrical power) is lacking. While they do not capture local conditions such as small terrain features and man-made structures, numerical simulations offer many advantages over direct measurements. Numerical simulations can provide a three-dimensional description of C_n^2

over regions of interest, simulations that can be performed anywhere on Earth at any time, and the ability to provide forecasts of OT that can be used for observational scheduling purposes. The quality of these types of simulations for describing the climatology of OT has recently been shown to be quite accurate (see reference [8]).

Although simulated climatologies of OT have great value for initial site selection and perhaps adaptive optics design, it is recommended that in-situ observations be available to better characterize local nature of OT at OGS. In addition, local data collection is needed in real-time systems to describe the performance of the link. This information is often useful in diagnosing performance issues and can provide inputs to support variable or adaptive coding and modulation techniques.

2.2.4 AEROSOLS

Aerosols are minute particles suspended in the atmosphere. They vary in size, concentration, and origin depending on the location on Earth, season, time of day, weather conditions, and natural events. Sources of aerosols include volcanic eruptions, desert dust, and human activities. Aerosols attenuate optical transmissions from satellites to the ground and must be accounted for in an optical communication system's link budget. Moreover, aerosols diffuse daytime Sun irradiance generating background sky radiance that can affect the performance of the optical link (see 3.4.2).

In general, transmission loss due to aerosol attenuation at most locations is less than 0.5–1 dB at wavelengths of 1060 and 1550 nm. To illustrate this effect, data were obtained from the Aerosol Robotic Network (AERONET) database (see reference [9]) for several urban locations and astronomical observatories around the globe and scaled to wavelengths of 1550 nm and 1060 nm. In urban locations, aerosols can be considered as a mixture of combustion byproducts, water molecules, and industrial pollutants. The data in figure 2-5 span a twenty-year period and include nearly 15 million total observations. The Cumulative Distribution Functions (CDFs) (see figure 2-5) show the median transmission loss due to aerosols for locations worldwide (black line) is about 0.21 dB at 1550 nm and 0.4 dB at 1060 nm. Transmission losses are less than 1 dB about 90 percent of the time at 1550 nm, and about 80 percent of the time at 1060 nm. However, there is considerable variation in the distributions by location. Mauna Loa Observatory by far is the cleanest atmosphere with a median transmission loss of less than 0.05 dB for both 1550 nm and 1060 nm. Izana, in the Canary Islands, has similar distributions to Mauna Loa Observatory; however, the distributions have longer tails because of the occurrence of the Calima events observed during late spring and summer. Beijing has the most severe aerosol extinction, with aerosol transmission losses routinely exceeding several dB regardless of wavelength. Similar measurements should be taken at OGS to quantify the distributions of aerosol transmission losses at those locations. The measurements can be used to identify the probability of severe attenuation (e.g., more than 1 dB) due to aerosols at each location and to adjust the link budget or to develop mitigation strategies to account for such events. All data is scaled to zenith; therefore transmission losses will be double at an elevation angle of 30 degrees.

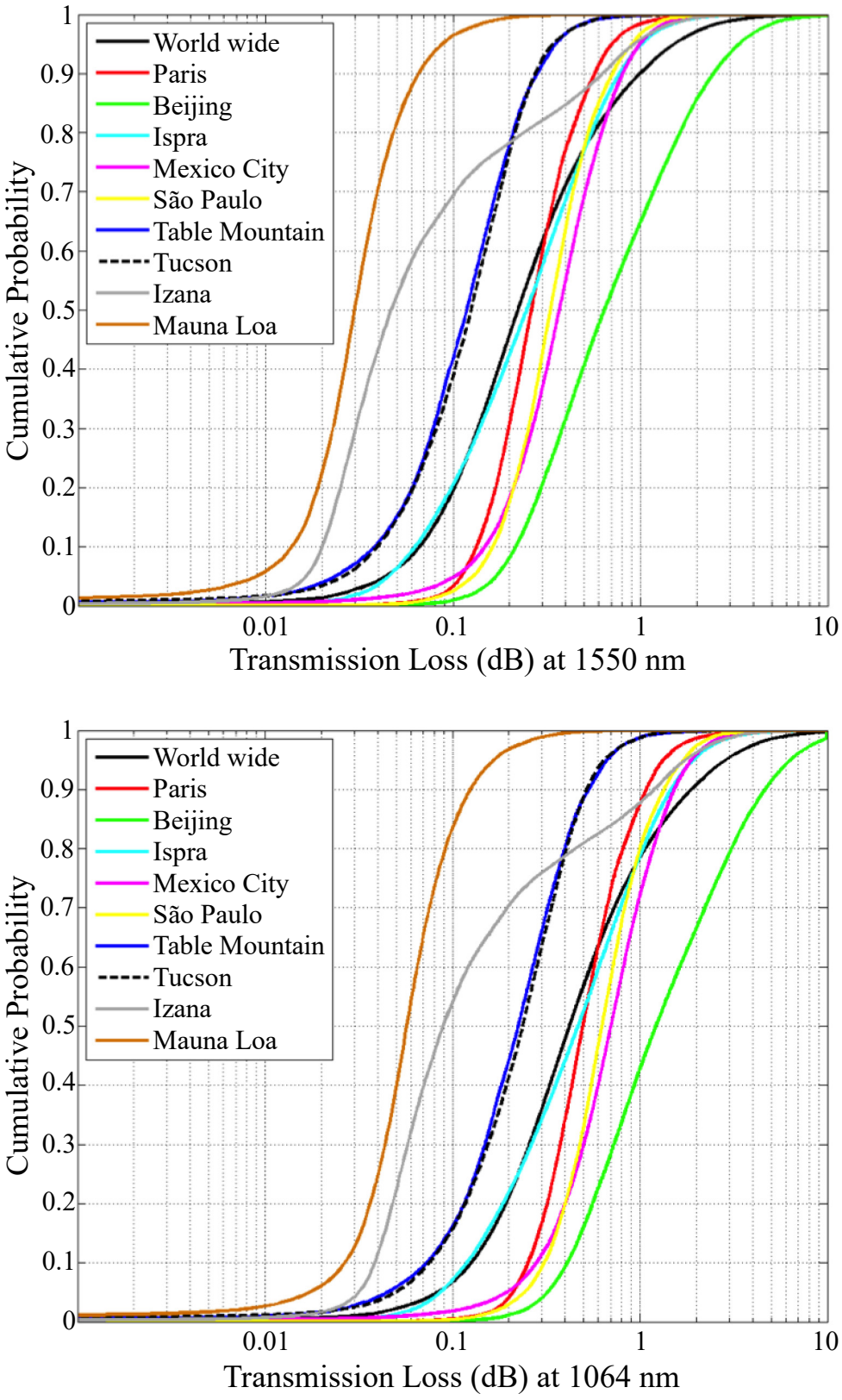

Figure 2-5: Transmission Loss

NOTE – Figure 2-5 shows transmission loss (dB), in the absence of clouds, scaled to 1550 nm (top) and 1060 nm (bottom) for several urban locations and astronomical observatories. The data shown were obtained from the AERONET database. Nearly 15 million observations were processed for the worldwide CDF with the data spanning over 20 years.

2.2.5 STANDARD METEOROLOGICAL QUANTITIES

Meteorological conditions must be considered in the design and operation of optical communications systems. Over the course of a year, or years, weather conditions can vary significantly at any particular location. Equipment must be designed and built to withstand the meteorological conditions at each site, which may involve large temperature and wind speed variations. Plans should be made to mitigate the risk of condensation on the equipment.

3 PHYSICAL QUANTITIES TO BE MEASURED OR DERIVED

3.1 INTRODUCTION

This section presents the physical quantities to be measured or derived for characterization of the critical atmospheric parameters (clouds, OT, aerosols, and standard meteorological quantities) affecting the quality of optical communication links. These physical quantities provide basic information regarding the atmospheric path quality, and measuring them or deriving their values is essential for link quality estimation and proper system operation, as well as long-term site characterization.

There are also certain additional quantities, including Rayleigh scattering, molecular absorption, scintillation, the particle distribution, and surface contamination that can be used for general characterization of the optical channel at a given site. Periodic measurements of these factors over long intervals of time (months or years) can facilitate identification of changes in the optical path characteristics. These quantities are not critical for system operation, however, and they are considered optional. Such additional quantities are discussed in annex A.

Table 3-1 summarizes the quantities considered in section 3 of this book; corresponding instruments to measure these quantities are described in section 4.

Table 3-1: The Physical Quantities and Instruments to Measure Them

Quantity	Subsection	Quantity Characteristics	Measurement Instrument/Derivation	Subsection
Clouds	3.2.2	Cloud Coverage	Whole Sky Image	4.2.1
	3.2.3	Cloud Base Height	Ceilometer	4.2.2
	3.2.4	Cloud Attenuation	Derived from Whole Sky Imager and Ceilometer data	4.2.1 and 4.2.2
Optical Turbulence	3.3.2	Atmospheric Coherence Length (Fried parameter)	Differential Image Motion Monitor	4.3.1
	3.3.3	Isoplanatic Angle	Derived from Differential Image Motion Monitor data	4.3.1-
Aerosols	3.4.1	Aerosol Attenuation	Sun Photometer	4.4.1
	3.4.2	Sky Radiance		
Standard Meteorological Quantities	3.5.1	Temperature	Thermometer	4.5.1
	3.5.2.	Wind	Anemometer/Anemoscope	4.5.2
	3.5.3	Pressure	Barometer	4.5.3
	3.5.4	Relative Humidity	Hygrometer	4.5.4

3.2 CLOUDS

3.2.1 GENERAL

Clouds strongly affect the optical communications signal strength, and the signal attenuation they cause varies widely with the cloud content (water or ice) and physical thickness of the clouds. Of main interest for optical communication links are cloud coverage, cloud attenuation, and cloud base height.

3.2.2 CLOUD COVERAGE

Closing an optical link requires a cloud-free line of sight. The amount of sky covered by clouds determines the desirability of using that site for a downlink. Therefore frequent measurements of cloud coverage from a Whole Sky Imager (see 4.2.1) are critical to the practical use of an OGS.

3.2.3 CLOUD BASE HEIGHT

The bases of clouds in a cloud mass are generally at the same height, because base height depends on the thermodynamic properties of the cloud mass, which are relatively homogenous spatially. Therefore cloud height is described using cloud base height instead of the height of the cloud tops, which significantly varies for different clouds. The cloud base height can be defined as the lowest altitude of the cloud. It is expressed in meters above the ground level or as the corresponding pressure level in hectopascal (hPa, equivalent to millibar).

Cloud base height can be used as an input, along with cloud particle backscatter information, to derive the optical loss that a laser beam can experience during propagation. The phase of the cloud (i.e., whether the cloud is composed of liquid water, ice, or both) influences its attenuation and is dependent on its height. Cloud base height and phase of the cloud are measured by a ceilometer (see 4.2.2).

3.2.4 CLOUD ATTENUATION

Clouds cause very high attenuation in optical links because they consist entirely of small water droplets and/or ice crystals, generally less than 0.01 cm in diameter (see reference [10]) that scatter and absorb optical wavelengths. Thus clouds can cause link fading for very long periods of time (hours or even days). There are a few exceptions where clouds produce minor attenuation (e.g., cirrus clouds) but even in such cases the attenuation fluctuations in time are strong enough to interfere with optical communication (see reference [10]). Apart from the physical thickness of the clouds, which varies widely with the cloud type and fluctuates in time, the cloud contents play a critical role in the attenuation. Typically, a water-based cloud will cause a 10 dB loss or more, while an ice-based cloud will cause a loss of approximately 1–8 dB (see figure 2-3). Therefore the cloud attenuation parameter is extremely important for estimating link availability and handover decision making between sites within a network.

Cloud attenuation can be derived using data from a ceilometer combined with data from an infrared whole sky imager (see reference [11]).

Another effect caused by the presence of clouds during an optical communication link is an increase in the sky radiance during the daytime. Clouds scatter the Sun irradiance and generate additional sky radiance compared to the amount that one would observe in clear sky conditions. While sky radiance may not adversely impact the quality of an optical link in a high photon flux regime, in a low photon flux regime, the consequence of additional sky radiance due to cloud scattering can be detrimental, resulting in a lower receiver signal-to-noise ratio (see 3.3.3).

3.3 OPTICAL TURBULENCE (ATMOSPHERIC SEEING PARAMETERS)

3.3.1 GENERAL

As a laser beam propagates through the atmosphere, its wavefront experiences distortions due to inhomogeneities in the index of refraction of the air, which are caused by variations in the temperature and pressure. These effects on an optical system can be quantified by atmospheric seeing parameters such as the atmospheric coherence length (Fried parameter) and isoplanatic angle (see reference [5]). The atmospheric seeing parameters can be computed using the profile of C_n^2, when it is known. However, the profile of C_n^2 is very impractical to measure and therefore the atmospheric seeing parameters are more easily measured by specially designed instruments which are described in section 4. The theory upon which the atmospheric seeing parameters is based is described in the following subsections.

3.3.2 ATMOSPHERIC COHERENCE LENGTH (FRIED PARAMETER, r_0)

The random phase aberrations of the wavefront in the receiving plane can be characterized by the Fried parameter, r_0, which is a quantitative measure of the quality of optical transmission through the atmosphere. The Fried parameter describes the diameter of a circle over which the root mean square wavefront aberration due to atmospheric optical turbulence is equal to 1 radian. The Fried parameter (see references [12] and [5]) is typically expressed in cm and can be defined as (see reference [13]):

$$r_0 = \left[0.423k^2 \sec(\xi) \int C_n^2(z)\, dz \right]^{-3/5}, \tag{1}$$

where ξ is the zenith angle (ξ=0 at the zenith and $\pi/2$ at the horizon) and $k=2\pi/\lambda$, [m^{-1}], is the wave number for a given wavelength λ, [m]. Equation (1) is valid from zenith down to approximately a 70-degree zenith angle. Although r_0 varies as a function of wavelength, it is typically referenced at a wavelength of 500 nm at zenith and then scaled according to the desired zenith angle and optical link wavelength.

When r_0 is much larger than a telescope aperture (D), the Full Width Half Maximum (FWHM) of the telescope Point Spread Function (PSF) is given by the diffraction limit of the telescope,

$$\theta_{DL} = \frac{\lambda}{D}. \tag{2}$$

Conversely, when r_0 is much smaller than the telescope aperture ($r_0 << D$) the aberrations caused by the optical turbulence prevents a telescope from approaching its diffraction limit. In this case, the FWHM of the telescope PSF, θ_T, is given by (see reference [14]):

$$\theta_T = 0.98\frac{\lambda}{r_o}. \tag{3}$$

Equation (3) indicates that the degradation due to optical turbulence may limit the ability of an optical system to focus the downlink optical power to a small detector area. This effect can impact the link data rate and signal loss unless solutions like adaptive optics, large area detectors, or arrayed detectors are employed.

Measurements and simulations of r_0 at locations considered for optical communications range from a few centimeters during the day (when the thermal gradient in the atmosphere is largest because the solar heating of the ground is at its maximum) to many tens of centimeters at night (see reference [8]).

The Fried parameter can be determined using measurements from a DIMM (see 4.3.1).

3.3.3 ISOPLANATIC ANGLE

The isoplanatic angle plays an important role in optical communication systems that use adaptive optics to correct the downlink and/or uplink signal. For instance, in some applications (e.g., GEO to Earth) adaptive optics corrections derived from a satellite downlink beam can be used to compensate for some of the distortions of the ground station uplink beam resulting from optical turbulence. To properly correct the uplink signal, the angular separation between the uplink beam and downlink beam must be less than the isoplanatic angle.

The region of the sky over which the turbulence pattern is temporally coherent is called the isoplanatic patch. For a ground telescope, the isoplanatic patch is described angularly by the isoplanatic angle, given by (see reference [15]):

$$\theta_{IS0} = 0.314\cos(\xi)\frac{r_o}{H} \quad \text{[rad]}, \tag{4}$$

where H [m] can be defined as the average turbulence altitude, defined as:

$$H = \left[\int C_n^2(z) z^{5/3} dz \Big/ \int C_n^2(z) dz\right]^{3/5}. \tag{5}$$

Equation (4) is valid from zenith down to approximately a 70-degree zenith angle.

If the Fried parameter and the profile of C_n^2 are available, the isoplanatic angle can be derived by equations (4) and (5). If the profile of C_n^2 is not available, it may be approximated by fitting existing C_n^2 models, such as the Huffnagel-Valley model (see reference [16]), that can provide the same measured Fried parameter.

Direct measurement of the isoplanatic angle may be obtained from an isoplanometer (see reference [17]); otherwise, values of θ_{ISO} can be derived from DIMM data (see reference [18]).

3.4 AEROSOLS

3.4.1 AEROSOL ATTENUATION

When a laser beam propagates from ground to space (and vice versa), the signal power is attenuated. The attenuation is the combined result of scattering and absorption by the molecules of the constituent gases of the atmosphere and aerosols suspended in the atmosphere, and is described by Beer's law:

$$I_t(\lambda_i) = I_o(\lambda_i)\exp\left(-\tau(\lambda_i)m\right), \tag{6}$$

where λ_i is the wavelength of interest, $I_t(\lambda_i)$ is the irradiance after a certain propagation path, $I_o(\lambda_i)$ is the initial signal irradiance, $\tau(\lambda_i)$ is the total atmospheric optical depth (or atmospheric optical thickness), and m is the air mass defined for a slant path with a zenith angle ξ as

$$m = sec(\xi). \tag{7}$$

Equation (7) is accurate for a zenith angle ξ up to 70 degrees, according to the parallel-plane atmosphere model. The slant path is critical since many space-to-ground optical communication systems will be operating at zenith angles greater than 0.0 degrees.

Since the total atmospheric optical depth, τ, is comprised of the effects of absorption and scattering by atmospheric gases and aerosols, one can write

$$\tau(\lambda_i) = \tau_a^s(\lambda_i) + \tau_a^a(\lambda_i) + \tau_m^s(\lambda_i) + \tau_m^a(\lambda_i), \tag{8}$$

where $\tau_a{}^s(\lambda_i)$ is optical depth due to aerosol scattering, $\tau_a^a(\lambda_i)$ is due to aerosol absorption, $\tau_m^s(\lambda_i)$ is due to molecular scattering, and $\tau_m^a(\lambda_i)$ is due to molecular absorption. The contribution of aerosols to the total extinction can be quantified by the aerosol optical depth, τ_a, defined as the sum of $\tau_a^s(\lambda_i)$ and $\tau_a^a(\lambda_i)$.

The fraction of the radiation that survives propagation through the atmosphere is called atmospheric transmittance, $T(\lambda_i)$, and is related to the total atmospheric optical depth as:

$$T(\lambda_i) = \exp\left(-\tau(\lambda_i)\right). \tag{9}$$

The atmospheric transmittance varies greatly over the optical spectrum because of the various contributions of the components of the atmosphere to the total optical depth as shown in equation (8). This spectral variation of the atmospheric transmittance is illustrated in figure 3-1, which depicts the total atmospheric transmittance over a wavelength range between 320 nm (UltraViolet [UV] range) and 1700 nm (InfraRed [IR] range). The data in the plot were generated using a radiative transfer code called MODerate resolution atmospheric TRANsmission (MODTRAN) (see reference [19]). In the plot, the blue line represents the total atmospheric transmittance and the red line shows the contribution to atmospheric transmittance by aerosols only. The wavelengths discussed in this book (1060 nm and 1550 nm) were chosen, in part, because of the small amount of extinction due to constituent atmospheric gases at those two bands. At these wavelengths, aerosol attenuation is the major component of the total atmospheric extinction. However, measurements show that the impact on optical communication systems is expected to be less than 1 dB 95 percent of the time (see figure 3-1).

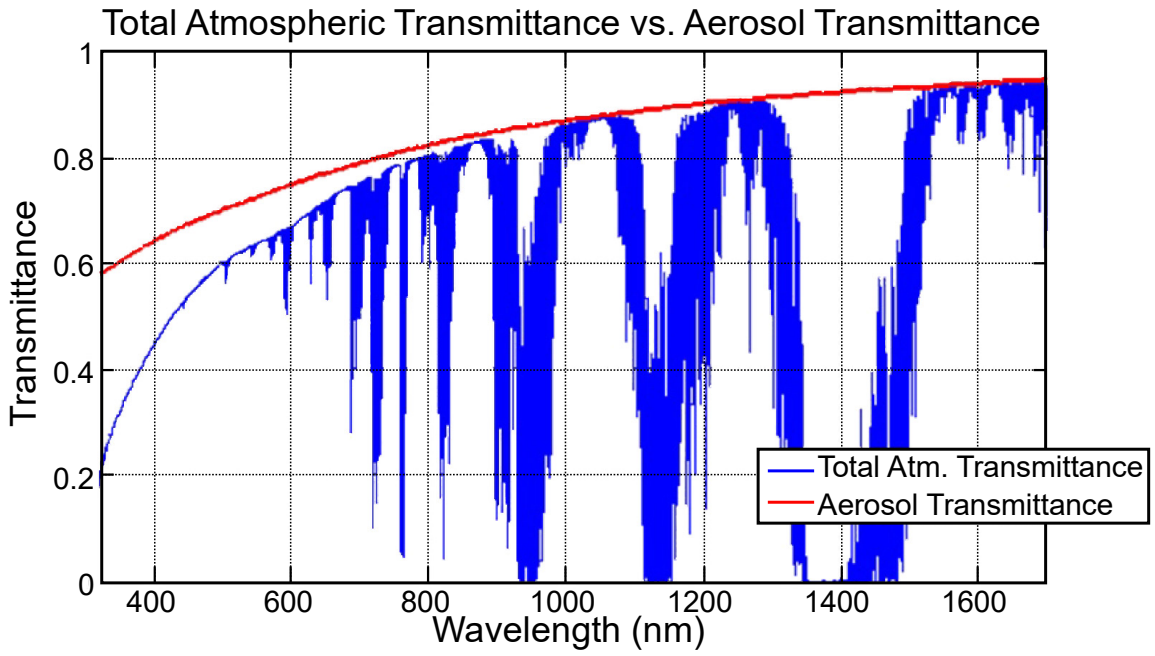

Figure 3-1: Example of Spectrum of Total Atmospheric Transmittance and Aerosol Transmittance

In figure 3-1, the curves describe a ground-to-space scenario at zenith. The ground station is at sea level with clear sky and rural aerosol distribution. The curves are obtained by computer simulations using the radiative transfer code MODTRAN.

Aerosol concentration and content experience a degree of variation during the day and the year because of the different meteorological conditions. Therefore it is desirable to monitor the aerosol optical depth and aerosol concentration at the site of a ground station to understand the atmospheric transmittance during operations and for site characterization (see reference [20]).

Aerosol attenuation can be calculated using measurements from a Sun photometer.

3.4.2 SKY RADIANCE

Daytime sky radiance is caused by the scattering of sunlight by the gasses and the aerosols suspended in the atmosphere. In the daytime, an optical receiver detects photons originated by sky radiance, which results in degradation of the Signal-to-Noise Ratio (SNR). SNR reduction due to sky radiance can be particularly detrimental to the link performance in a low photon flux regime link operation, such as an optical deep space link (see references [21] and [22]). Therefore the characterization and calculation of the sky background noise power originated by the sky radiance is recommended for those scenarios.

Sky radiance, $L_\lambda(\lambda_i)$, is usually described with units of [W/cm^2/sr/μm] or [μW/cm^2/sr/nm]. Values of daytime sky radiance greatly vary under different conditions, particularly depending on the angular distance between the observer and the Sun disk; however, statistical analysis of ground measurements and simulation results from atmospheric radiative transfer software programs such as MODTRAN can provide an assessment of the expected sky radiance.

The strength of sky radiance is dependent on the separation angle between the receiver station observation angle and the Sun, and increases as the separation angle decreases. Typically, sky radiance may increase with larger zenith angles and with increasing aerosol concentrations (see reference [23]).

The sky background noise power, $P_t(\lambda_i)$, collected by the ground receiver, given a sky radiance $L_\lambda(\lambda_i)$ is

$$P_t\left(\lambda_i\right) = L_\lambda\left(\lambda_i\right) A \Delta\lambda \Omega_r \eta_s \,, \tag{10}$$

where A is the receiver (or telescope) area, $\Delta\lambda$ is the receiver's spectral bandpass, Ω_r is the solid angle of the receiver's field of view, and η_s is the system optical efficiency (or optical loss) (see reference [24]).

Although sky radiance can be determined using measurements from a Sun photometer, atmospheric radiative transfer software programs such as MODTRAN can also provide adequate estimates for link budget purposes.

3.5 STANDARD METEOROLOGICAL QUANTITIES

3.5.1 TEMPERATURE

The temperature variations in the air are the main cause of optical turbulence Also, atmospheric temperature is used to determine cloud composition (water or ice), which, in turn, is used to estimate the signal attenuation produced by the clouds. Finally, extreme air temperatures may affect the design of optical ground stations and/or influence ground station operations. Temperature is measured using a thermometer.

3.5.2 WIND

Wind is an important parameter affecting laser communications because it constantly moves the air masses. Together with the satellite movement, the wind causes changes in the optical turbulence profile along the propagation path. These changes lead to fluctuations in the optical signal level. Furthermore, wind is the main cause of cloud movement that could lead to changes in the cloud coverage over time. Finally, some ground station locations may experience strong wind speeds that can cause movement and vibrations in optical receivers and even damage ground station components (such as the telescope dome). Therefore wind characteristics (speed and direction) must be considered in the physical design and construction of optical ground stations. Wind direction is usually expressed in terms of the direction from which it originates and is reported in cardinal directions (e.g., N, NE, SW, etc.) or in azimuth degrees. Surface wind speed is reported globally at a height of 10 meters above ground in km/h, knots, or m/s.

Wind direction and speed are measured with an anemoscope and an anemometer, respectively.

3.5.3 PRESSURE

Atmospheric pressure is the force per unit area exerted on a surface by the weight of the air in the atmosphere above that surface. Atmospheric pressure depends on temperature and humidity and generally decreases with increasing altitude. Pressure is measured with a barometer.

3.5.4 RELATIVE HUMIDITY

Relative humidity is the ratio of the existing partial pressure of water vapor to the equilibrium vapor pressure at the same temperature. High relative humidity levels imply that the dew point (the saturation temperature for water in air) is close to the current air temperature, which can lead to condensation on the ground station’s equipment. To prevent such a situation, humidity levels should be monitored before and during operations so that proper action (such as station handover and closure of the telescope dome) can be initiated before critical levels are reached. Relative humidity is measured with a hygrometer.

4 INSTRUMENTS TO MEASURE PHYSICAL QUANTITIES

4.1 INTRODUCTION

This section serves as a guideline regarding instruments used to measure the primary physical quantities outlined in section 3. It provides examples of instruments currently in use. These specific instruments are not required, but each site should be sufficiently equipped to provide real-time measurements of the primary physical quantities. A recent example of many of the types of instruments listed below are shown in references [65], [4], and [67]. The Laser Communications Atmospheric Monitoring System leverages information contained in this green book.

4.2 CLOUDS

4.2.1 WHOLE SKY IMAGER

4.2.1.1 General

The Whole Sky Imager (WSI) is a passive (non-emissive) system that acquires images of the sky dome used for assessing and documenting cloud fields and cloud field dynamics. The received sky images can be used to evaluate the presence, distribution, shape, and radiance of clouds over the entire sky. In particular, the WSI is used to determine cloud coverage, and in conjunction with the ceilometer's backscatter profile of the cloud particles to estimate cloud attenuation. Two types of WSI are currently in use: visible and infrared.

4.2.1.2 Visible

The visible WSI provides cloud information during the day and has a fish eye lens with wide Field Of View (FOV) that focuses the whole sky image onto a Charge-Coupled Device (CCD) camera. To guarantee proper operation under all weather conditions, a closed module heater and cooling fan are implemented (figure 4-1). Figure 4-2 shows an example image from the WSI used in Japan's National Institute of Information and Communications Technology (NICT) weather monitoring system (see reference [4]). The characteristics of this WSI are listed in table 4-1.

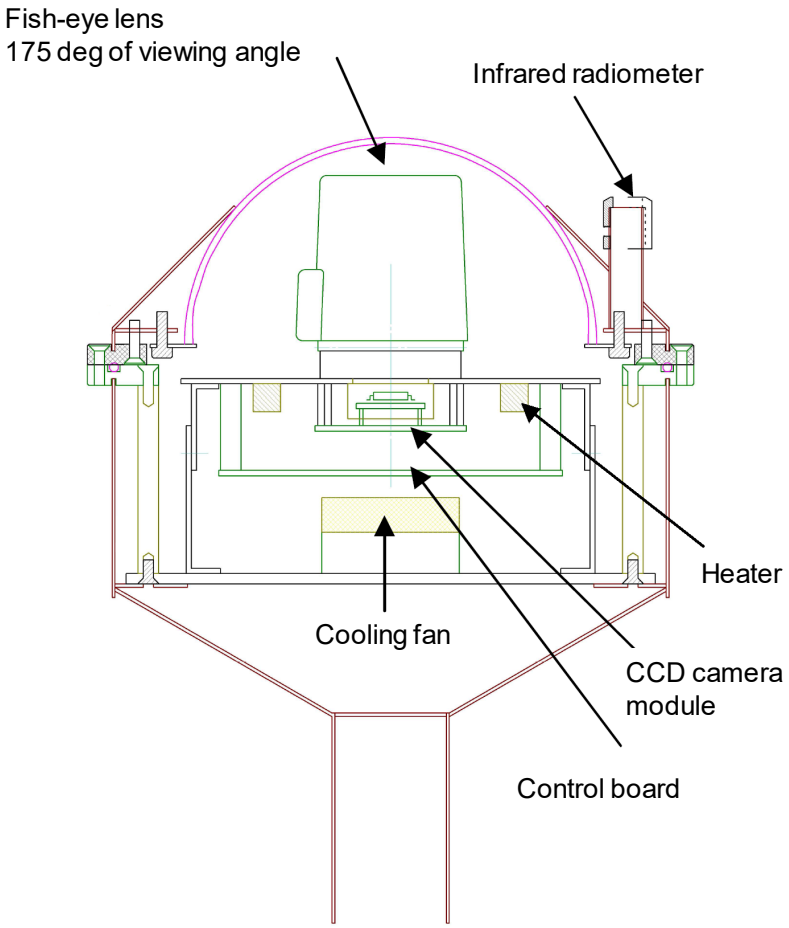

Figure 4-1: NICT Whole Sky Imager Structure

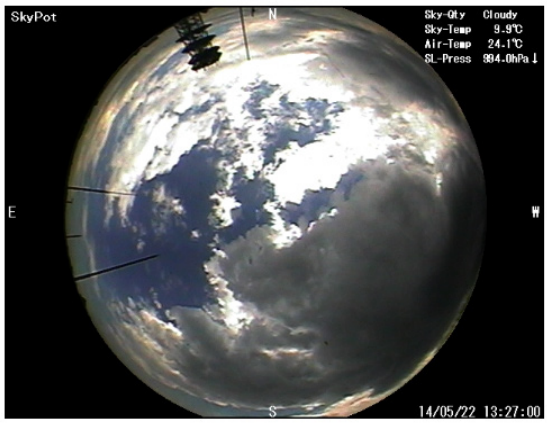

Figure 4-2: Example Image from the NICT Whole Sky Imager

Table 4-1: Characteristics of the NICT Whole Sky Imager

Parameter	Value
CCD number of pixels	4.1 Mpix (811(H) x 508(V))
CCD diagonal	1/2 inch
Fish-eye lens field of view	185 degrees

4.2.1.3 Infrared

An IR detector (an uncooled microbolometer array) and a fish-eye lens with a 180-degree field of view could also be used for cloud imaging in the thermal IR during both night and day. An example of such an instrument recently installed at the European Space Agency's (ESA's) deep-space station in Cebreros, Spain, is shown in figure 4-3. A schematic overview of its specifications is presented in figure 4-4.

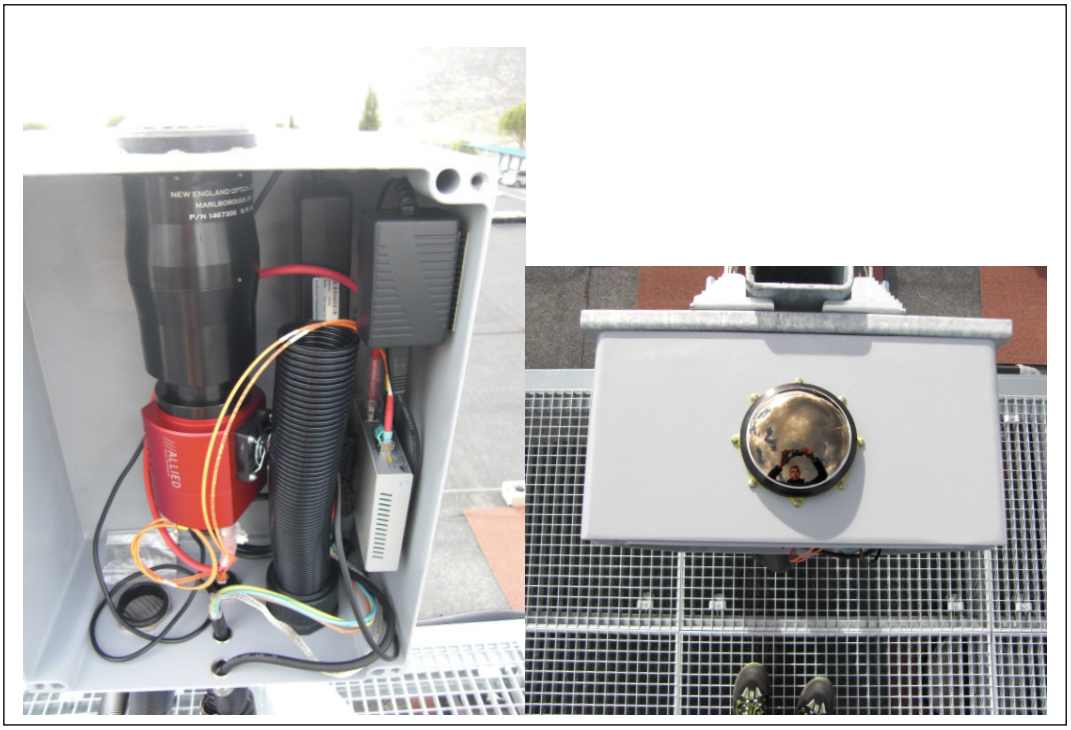

Figure 4-3: ESA Thermal Infrared Cloud Sensor

NOTE – In figure 4-3, the left image shows the open enclosure, with the fish-eye lens (black) at the left and the Commercial Off-The-Shelf (COTS) thermal IR sensor (red) attached below. The corrugated black tube serves to duct cooled dry air into the enclosure to maintain temperatures at suitable operating levels. The image on right shows the fish-eye lens from above. The front germanium element is not transparent in the visible.

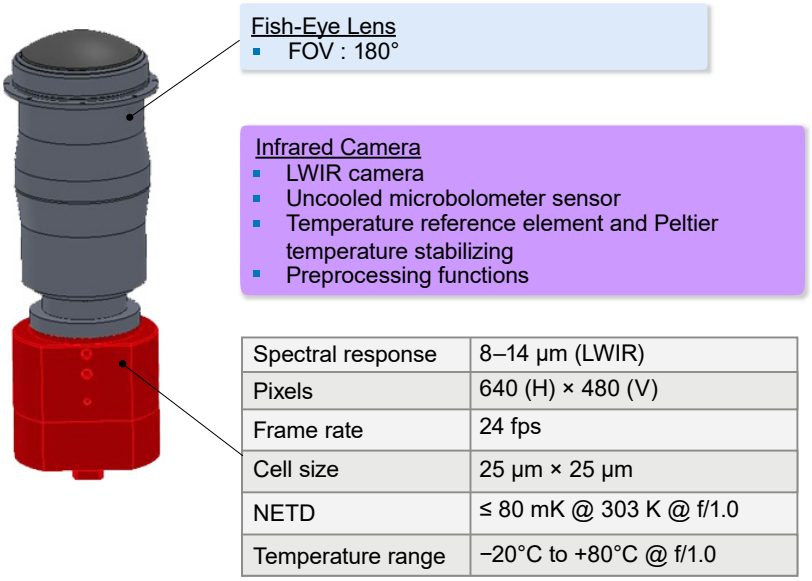

Spectral response	8–14 µm (LWIR)
Pixels	640 (H) × 480 (V)
Frame rate	24 fps
Cell size	25 µm × 25 µm
NETD	≤ 80 mK @ 303 K @ f/1.0
Temperature range	−20°C to +80°C @ f/1.0

Figure 4-4: Components of ESA's IR Sky Dome Imager

A sample IR cloud image from the ESA instrument (taken while experimenting with the instrument on the roof of a building in Darmstadt, Germany) is shown in figure 4-5.

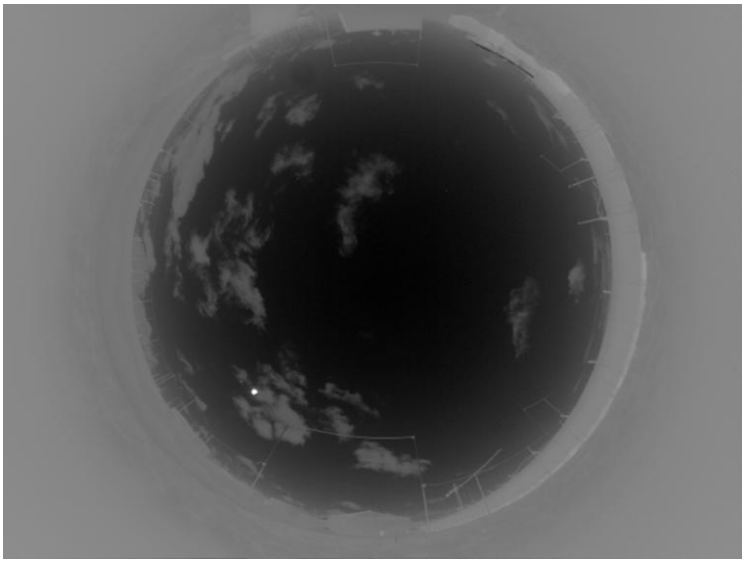

Figure 4-5: Sample Sky Image Taken by ESA's IR Sky Dome Imager

Another example of an IR cloud sensor is the NICT instrument shown in figure 4-6. It consists of five passive infrared temperature sensors that are pointed in the north, south, east, west, and vertical directions. Figure 4-7 shows the percentage of cloud coverage in each of the five areas, according to data received from the instrument shown in figure 4-6.

Figure 4-6: NICT Infrared Cloud Sensor

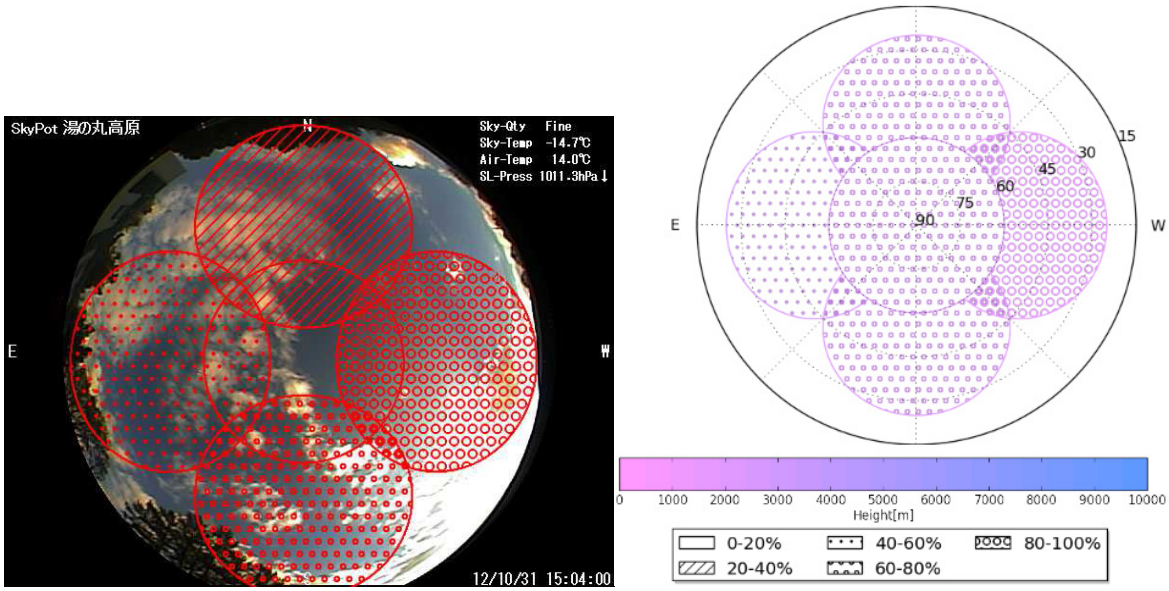

Figure 4-7: Cloud Coverage Diagram from the NICT IR Cloud Sensor

The structure of the NICT IR temperature sensor is shown in figure 4-8. The instrument has an internal thermometer and a connection to an external thermometer to measure the temperatures. It also has a heater to ensure equal temperatures inside the sensor and outside the system, which is important to guarantee suitable operation conditions for the front lens. The FOV of the IR sensor used in the NICT weather monitoring system is 60 degrees.

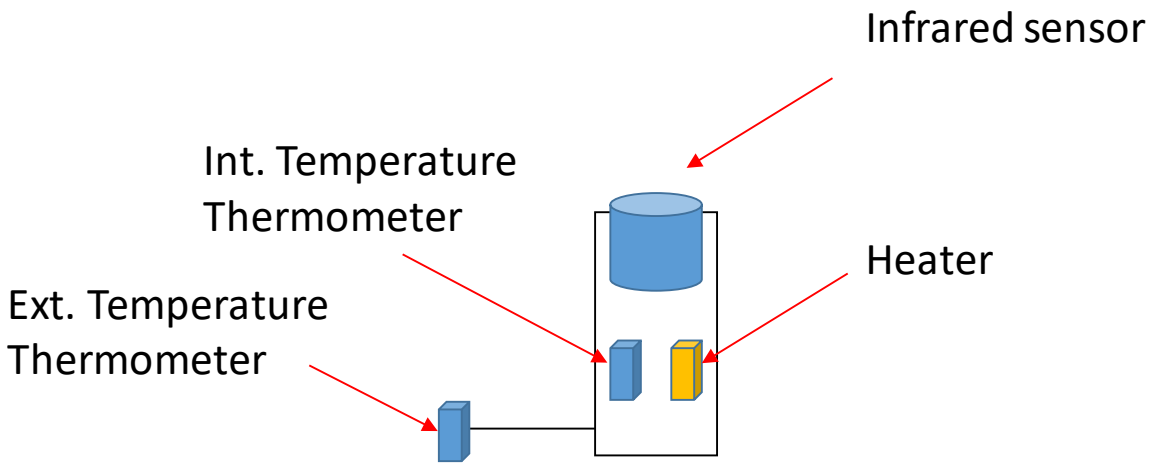

Figure 4-8: NICT IR Thermometer

Another example of an infrared WSI instrument is shown in figure 4-9 (see reference [25]). The All Sky Infrared Visible Analyzer (ASIVA) is a multi-purpose visible and infrared sky imaging and analysis instrument whose primary function is to provide radiometrically calibrated imagery in the mid-infrared (8-12 microns). This functionality enables the determination of diurnal hemispherical cloud fraction and estimates of sky/cloud temperature from which one can derive estimates of cloud emissivity and cloud height.

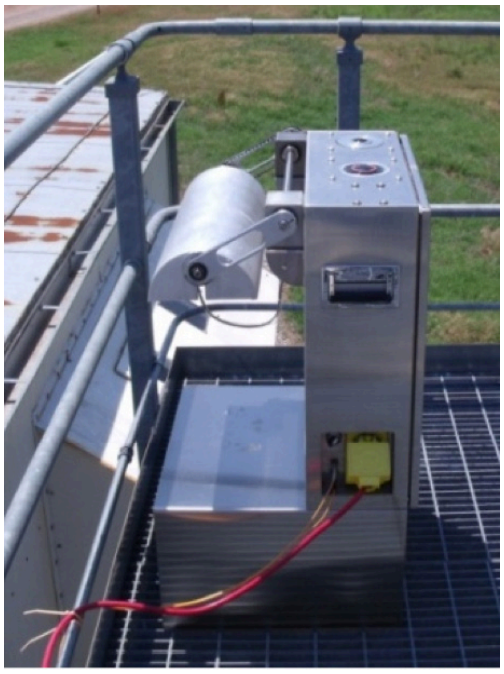

Figure 4-9: ASIVA Infrared Cloud Instrument

An example of output from the ASIVA is shown in figure 4-10.

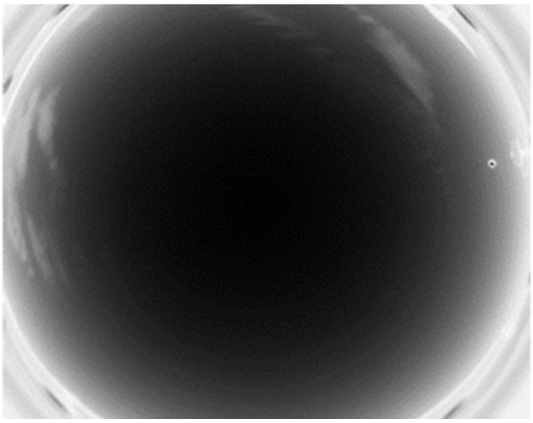

Figure 4-10: Infrared Image of Clouds from the ASIVA Instrument

In addition, the National Aeronautics and Space Administration (NASA) Jet Propulsion Laboratory (JPL) deployed two long-wave infrared-based (7.5-13.5 μm) cloud imaging systems at facilities in Table Mountain, CA and Goldstone, CA. These systems can continuously monitor the sky (day and night), providing highly stable and reliable data (see reference [26]). Each instrument consists of a 14-bit digital camera using an uncooled microbolometer detector array of 324 × 256 pixels with a system field of view up to 110 degrees. The system is protected by a weather-proof enclosure (see figure 4-11).

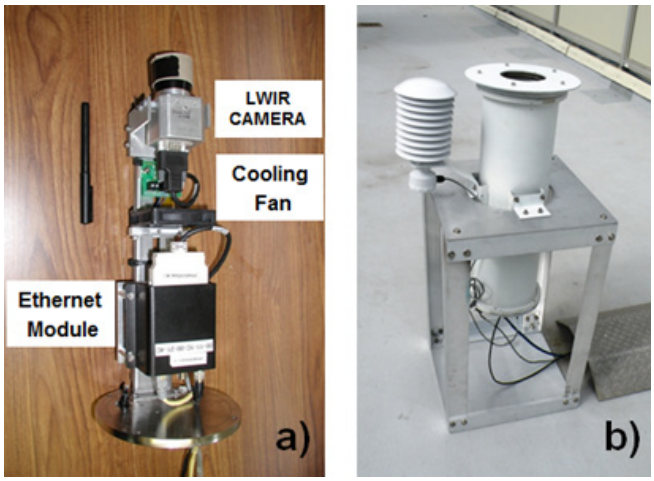

Figure 4-11: Cloud Imaging System

NOTE – Figure 4-11a) shows a NASA/JPL cloud imaging system, composed of a LongWave InfraRed (LWIR) camera, heater and cooling fan, and Ethernet module. Figure 4-11b) shows deployment of a cloud camera using a weather-proof enclosure that allows imaging of the sky via a germanium window.

Because the response of the camera's microbolometer array drifts with temperature, the images are corrected in real time to measure the overall downwelling sky radiance, while distinct dedicated algorithms correct the camera readings for other sources of noise (see reference [27]). Clouds are detected by subtracting the estimated atmospheric emission from

the downwelling sky radiance (see reference [28]) in such a way that cloud optical depth and attenuation can be determined by applying one or more thresholds to the residual radiance (see reference [11]).

Figure 4-12 shows an example of the processing of a sky image, with the overall downwelling sky radiance illustrated in figure 4-12a). After atmospheric emission removal and thresholding, the cloud map depicting the sky optical depth is indicated in figure 4-12b).

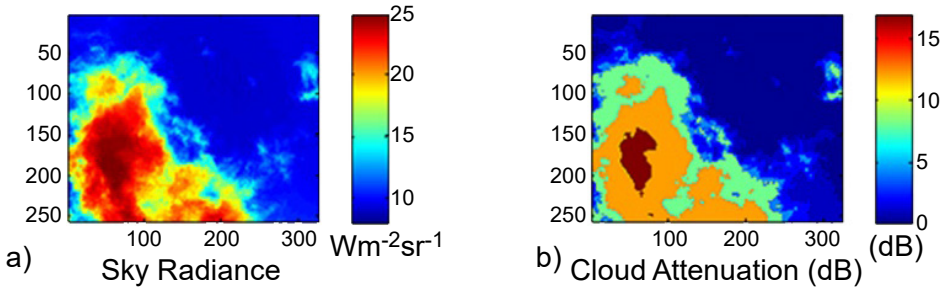

Figure 4-12: Example of Processing of the Sky Image from the NASA/JPL Cloud Imager

NOTE – Figure 4-12a) shows the overall integrated downwelling sky radiance, and Figure 4-12b) shows the cloud map with corresponding sky optical depth obtained after processing of the image.

4.2.2 CEILOMETER

The ceilometer is a device that uses a light source to determine cloud base height and to derive cloud attenuation (in conjunction with the WSI).

A laser ceilometer consists of a vertically pointing laser and a LIDAR receiver. The instrument sends a short laser pulse (about a nanosecond) through the atmosphere. The LIDAR receiver detects the returning light due to scattering by aerosols (Mie scattering). The height of the clouds is obtained by measuring the delay between the sent and returned signal. Such laser ceilometers are regularly used at airports and are compliant with eye-safety regulations (for example, see references [29] and [30]). An example of a ceilometer can be found in figure 4-13. Figure 4-14 shows the backscatter from a CL51 ceilometer as a function of height and time. Bright colors indicate strong backscatter, and thus possible clouds.

Figure 4-13: Example of a Vaisala Ceilometer, Which Measures Cloud Heights to 13 km

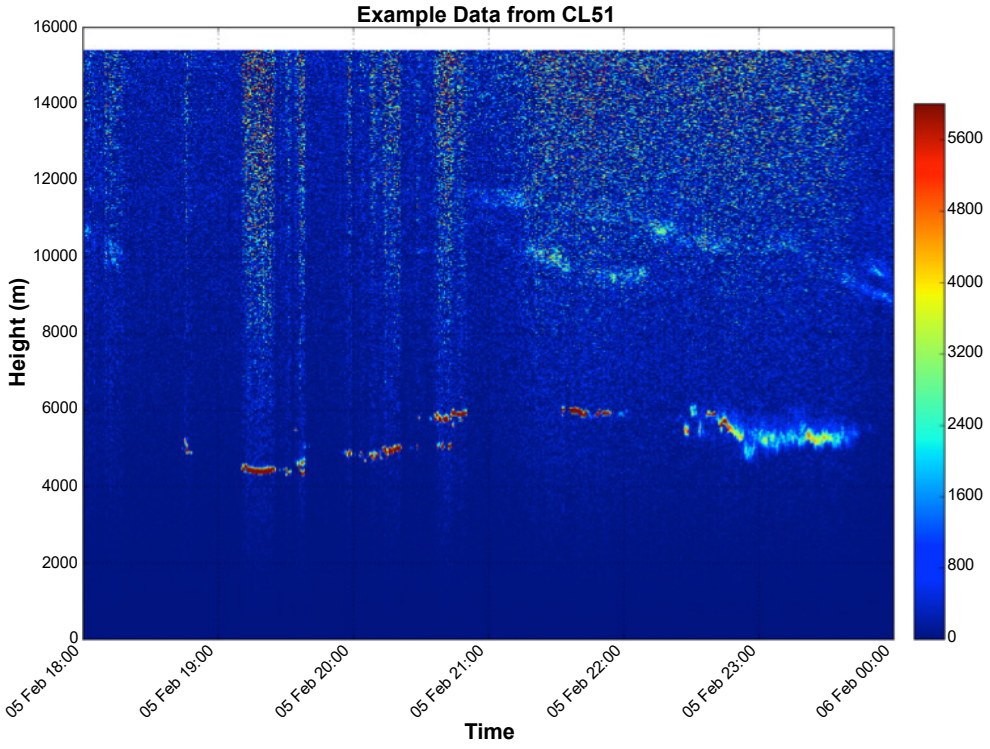

Figure 4-14: Backscatter from a Vaisala Ceilometer Showing Various Cloud Heights as a Function of Time

4.3 OPTICAL TURBULENCE (ATMOSPHERIC SEEING PARAMETERS)

4.3.1 DIFFERENTIAL IMAGE MOTION MONITOR

A DIMM is an instrument used to evaluate the seeing conditions at an OGS site. The results are presented in the form of atmospheric seeing [arcsec] or more often as the Fried parameter, r_0 [cm]. Figure 4-15 shows the structure of one possible DIMM system (see references [31] and [32]).

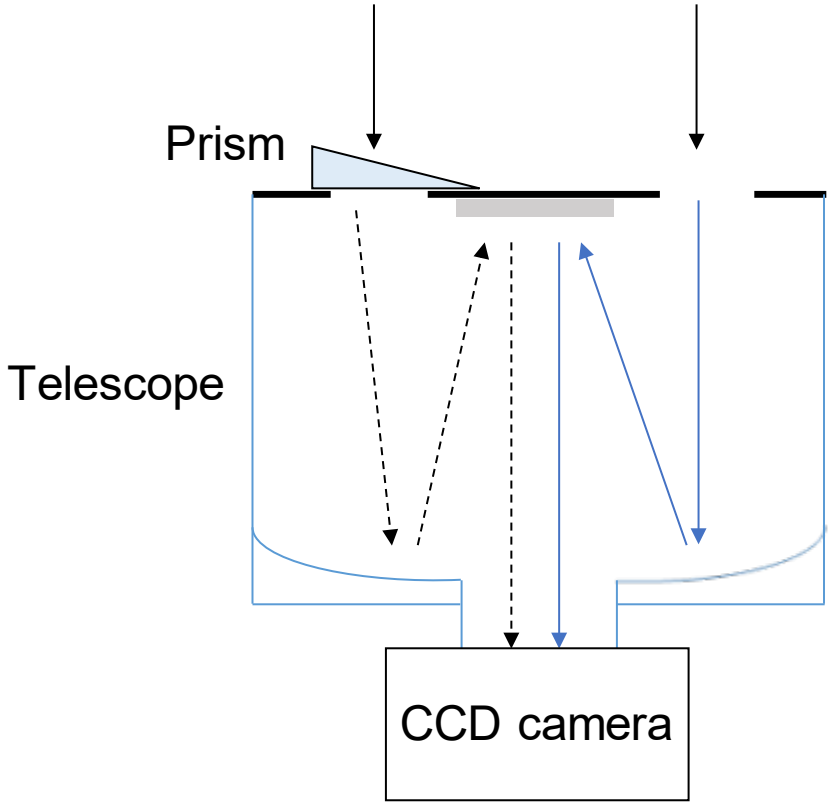

Figure 4-15: Example of a DIMM System

At the front of the telescope, a mask with two small apertures—one or both of them covered with optical prisms—is installed. The source can be a star or a downlink beam from a satellite. The light from the source is refracted by the prisms, and two images are obtained on the focal CCD camera.

The Fried parameter can be found by calculating the variance of the relative position of each centroid. However, there is a restriction on the Fried parameter values that such a setup can measure, depending on the size of the apertures and the distance between them. The measured variances of the differential motions of the two images of the source—σ_L (the projection parallel to the line connecting the apertures) and transverse σ_T (the projection perpendicular to the connecting line)—are related to the Fried parameter as:

$$\sigma_L^2 = 2\lambda^2 r_{0L}^{-3/5}\left(0.179 D_M{}^{-1/3} - 0.0968 d_a{}^{-1/3}\right) \text{ and} \tag{11}$$

$$\sigma_T^2 = 2\lambda^2 r_{0T}^{-3/5}\left(0.179 D_M{}^{-1/3} - 0.145 d_a{}^{-1/3}\right), \tag{12}$$

where r_{0L} is the Fried parameter in the longitudinal direction and r_{0T} is the Fried parameter in the transverse direction, d_a is the distance between the apertures, and D_M is the mask aperture diameter.

As an example, the parameters of the NICT DIMM used with light from a star/satellite are listed in table 4-2.

Table 4-2: NICT Setup Parameters

Telescope aperture	100 mm
Focal length	800 mm
Mask aperture diameter D_M	20 mm
Distance between apertures d_a	80 mm
Prism vertical angle	0.5 deg

During the daytime, atmospheric turbulence can become very pronounced as solar heating of the Earth surface causes a larger thermal gradient in the atmosphere profile. As a consequence of this process, the Fried parameter can reach values of as little as a few centimeters. In that case, measurements of the Fried parameter during daytime can be very critical for site characterization for daytime operations.

Another approach to measure the Fried parameter during the daytime is to use a Solar DIMM (SDIMM). An SDIMM uses the Sun as a source and operates according to principles similar to those of a DIMM: two sub-apertures over a telescope mask project two images of the Sun over a camera (see figure 4-16). The Fried parameter is derived by monitoring the differential motion of the limbs of the two images of the Sun (see reference [33]). An SDIMM was validated during the Advance Technology Solar Telescope (ATST) survey to determine most suitable site to locate the Daniel K. Inouye Solar Telescope (see reference [34]).

Figure 4-16: Example of Solar DIMM

NOTE – The instrument in figure 4-16 was deployed at the NASA/JPL's facility of Goldstone (CA). The instrument is built on a 16-inch telescope. The two sub-apertures used for differential imaging of the Sun disk are visible over the telescope mask.

4.4 AEROSOLS

4.4.1 SUN PHOTOMETER

A valid approach to measure the optical properties of the atmosphere is to directly monitor the variation the spectral irradiance of a known exo-atmospheric source. In particular, Sun photometry is a well-established remote sensing technique for the characterization of atmospheric optical properties, including aerosol attenuation, sky radiance, and particle distribution (see reference [11]).

The operation principles of a Sun photometer can be explained as follows. A sensor head mounted on a gimbal tracks the Sun and at given intervals of time takes measurements of the Sun's irradiance (direct Sun-pointing) and sky radiance (at well-defined off-pointing positions from the Sun) at different wavelengths. These wavelength channels are selected in a way such that they do not experience deep molecular absorption, and therefore the measured Sun irradiance only experiences extinction due to molecular scattering (which is approximately constant in time at the same location) and aerosols (whose concentration varies in time).

Generally, the collected solar flux that is measured by a Sun photometer provides a reading voltage as

$$V\left(t,\lambda_i\right)=C\left(\lambda_i\right)I_s\left(\lambda_i\right)\exp\left[-\left(\tau_m\left(\lambda_i\right)m+\tau_a\left(t,\lambda_i\right)m\right)\right], \tag{13}$$

where: λ_i is the wavelength (or channel) of interest, $V\left(t,\lambda_i\right)$ is the voltage read by the instrument, $C\left(\lambda_i\right)$ is a wavelength-dependent constant of the instrument, $I_s\left(\lambda_i\right)$ is the Sun's irradiance above atmosphere, $\tau_m\left(\lambda_i\right)$ is the optical depth (or atmospheric optical thickness) due to molecular scattering (Rayleigh scattering), $\tau_a\left(t,\lambda_i\right)$ is the optical depth related to the aerosol concentration, and *m* is the atmosphere air mass.

Assuming a well-calibrated instrument and that $\tau_m\left(\lambda_i\right)$ is constant in time, the only unknown is the optical depth, $\tau_a\left(t,\lambda_i\right)$; that is:

$$\tau_a\left(t,\lambda_i\right)=\frac{1}{m}\log\left(\frac{C\left(\lambda_i\right)I_s\left(\lambda_i\right)}{V\left(t,\lambda_i\right)}\right)-\tau_m\left(\lambda_i\right). \tag{14}$$

Once the optical depth is computed, atmospheric transmittance and thus signal fading can be computed using equation (9).

AERONET is an established network of Sun photometers. Figure 4-17 below shows an example of an AERONET Sun photometer. Example data from AERONET are shown in figure 2-5. (For more information on the specifics of this instrument, see reference [9].)

Figure 4-17: AERONET Sun-Photometer at NASA/JPL's Facility in Goldstone, CA

4.5 STANDARD METEOROLOGICAL QUANTITIES

4.5.1 THERMOMETER

Temperature sensors measure the amount of heat energy that is generated by an object or system and can provide an analog or digital output. There are several types of temperature sensors, for example, thermostats, thermistors, resistance temperature detectors, and thermocouples.

For example, the resistance temperature detector (Pt100) used by NICT can measure temperatures ranging between −60 and +60º C (±0.2º C @ 20º C).

4.5.2 ANEMOSCOPE/ANEMOMETER

An anemoscope is a device used to show the wind direction or to foretell a change of wind direction or weather. An anemometer is a device used to measure the wind speed. Figure 4-18 shows the anemometer/anemoscope at the NICT weather station. The anemoscope is set at 0 degrees when pointing north, at 90 degrees when pointing east, 180 degrees when pointing south, and 270 degrees when pointing west. It captures 16 different wind directions (N, NEN, NE, etc.) every 100 ms. The most frequent wind direction is saved at one-minute time intervals. Wind speed samples are taken every second and the average value is saved every minute. Because dome closures are required in high winds, it is important for the anemometer to measure wind speeds greater than the threshold of operations.

Figure 4-18: Anemometer/Anemoscope at NICT

4.5.3 BAROMETER

Many different types of barometers are used to measure pressure. For example, resonant and thermal sensors measure pressure by detecting changes in gas resonant frequency or thermal conductivity, respectively. Another type of pressure sensor uses a force collector to measure strain due to applied force over an area. Such sensors can be piezo-resistive strain gauge, capacitive, electromagnetic, optical, etc.

4.5.4 HYGROMETER

Relative Humidity (RH) is measured by a hygrometer. There are several different types of hygrometers, for example, psychrometers, mechanical hygrometers, electrical impedance hygrometers, dew-point RH hygrometers, and capacitive RH hygrometers.

5 TEMPORAL CONSIDERATIONS FOR THE COLLECTION OF PHYSICAL QUANTITIES

5.1 INTRODUCTION

As discussed in previous sections, certain atmospheric parameters can degrade or prevent optical communications links between satellites and ground stations. To minimize the impacts of atmospheric phenomena, it is critical to measure the physical quantities associated with these phenomena periodically. Long-term data collection, defined as data collected over a period of months to many years, is very important to the design of optical communications systems. Knowledge of the characteristics of clouds, including their diurnal, monthly, and seasonal behavior, can be used to estimate the expected performance of a system. Additionally, long-term cloud attenuation statistics can be used to improve link budget definitions. Similarly, long-term turbulence statistics may influence the design of the AO system or other turbulence mitigation strategies. Finally, long-term statistics of aerosol attenuation can be used to improve link budget calculations.

During operations, atmospheric measurements may be used to determine the site or sites to which a given satellite should attempt to send data. Sometimes it will be necessary to transfer (handover) the satellite laser communications transmission from one ground station to another. For example, if station A is receiving a downlink and is becoming cloudy, but station B is clear, it may be worthwhile to repoint the satellite transmitter to station B to minimize downtime. Similarly, sometimes it may be necessary to reduce the data rate during severe turbulence or aerosol events to achieve acceptable performance levels. It may also be necessary on occasion to close the dome and shut a ground station down to protect sensitive equipment or the physical structure from the effects of weather.

Since some atmospheric quantities change more rapidly than others, it is important to define how often these atmospheric data should be collected (i.e., the sampling rate) to support the operations of optical communications systems. The following subsections discuss considerations pertaining to the sampling rates for several atmospheric parameters. Long-term data collection is discussed first, followed by a discussion of data collection to support real-time operations. For many quantities, the sampling rates and measurement equipment and strategies are similar for long-term and real-time data collection, and data collected in real time may eventually become a long-term database. The recommendations in this report are based on current knowledge and experience, but actual sampling rates may depend on the system Concept of Operations (CONOPS).

5.2 LONG-TERM COLLECTION

5.2.1 MINUTES TO AN HOUR

5.2.1.1 Cloud Coverage

Clouds can range in size from less than one kilometer to several thousands of kilometers. Sometimes they are very persistent and other times they evolve rapidly. Since clouds can be

blown quickly by the wind, and can change size and shape rapidly, they should be measured every few minutes. For long-term characterization the sampling rate should be on the order of minutes with the sampling rate not less than once per hour.

5.2.1.2 Cloud Base Height

The height of the base of a cloud can be used to help determine its attenuation based on its temperature and whether it is composed of water or ice. Cloud base height generally changes slowly, and long-term statistics can be developed with a measurement sampling rate on the order of minutes.

5.2.1.3 Cloud Attenuation

It is possible, but not necessarily desirable, to communicate through some thin clouds. Long-term collection of cloud attenuation data can help quantify how often communication through clouds is feasible. This analysis could lead to the inclusion of additional link margin in a system if it is determined to have a significant impact on system availability. As clouds move and evolve over time, the attenuation of the signal changes on the order of minutes. In addition, the structure of clouds is inhomogeneous, and some areas within the same cloud can attenuate the signal more or less than other areas. To capture these characteristics, cloud attenuation should be measured on the order of minutes, not to exceed one hour (see reference [11]).

5.2.1.4 Aerosol Attenuation, Sky Radiance, and Particle Distribution

Significant changes in atmospheric attenuation due to aerosols generally occur on time scales much longer than minutes. Similarly, sky radiance does not vary significantly from minute to minute. Therefore long-term collection of these data types can be performed with sampling rates on the order of once per hour.

5.2.1.5 Standard Meteorological Quantities

It is important to know the long-term statistics of standard meteorological quantities (temperature, wind, pressure, relative humidity) at OGS. Knowledge of these quantities is required to design a system that can operate safely and accurately in the common weather conditions that occur at a site. It is also important to understand how often it may be necessary to close a ground station under certain conditions (e.g., precipitation, fog, high winds) to protect its sophisticated components. These standard parameters can change on the order of minutes, but for long-term collection, a sampling rate of minutes to as long as one hour is sufficient to develop good distributions.

5.2.1.6 Optical Turbulence (Atmospheric Seeing Parameters)

Optical turbulence occurs on small spatial and temporal scales, and varies much more rapidly than the other parameters discussed in this Report. Although an operational communications system may have to compensate for the effects of turbulence on time scales as small as milliseconds, it is sufficient to measure the OT parameters (Fried coherence length [r_0], scintillation, and isoplanatic angle) for long-term characterization on the order of one minute to a few minutes. Taken over all times of year and all times of day, data at this rate should provide an accurate distribution of the optical turbulence parameters.

5.2.2 SECONDS TO MINUTES

There are no parameters that are recommended to be measured at a sampling rate of seconds to minutes for long-term data collection.

5.3 REAL-TIME COLLECTION

5.3.1 MINUTES TO AN HOUR

5.3.1.1 Cloud Coverage

Clouds produce the largest fades in optical links and are the most important atmospheric quantity to mitigate for successful optical communication systems. Clouds can be blown quickly by the wind, often moving in and out of the line of sight of an optical link. Similarly, clouds can form and dissipate rapidly, with these processes occurring on time scales on the order of minutes. Therefore a ground-based cloud sensor is required to characterize small-scale cloud features and the potential rapid evolution of clouds above ground stations. The cloud data should be collected at time scales on the order of minutes.

5.3.1.2 Cloud Base Height

Although not as important as cloud attenuation, the cloud base height is another measurement to collect on time scales between several minutes and an hour.

5.3.1.3 Cloud Attenuation

A measure of the attenuation due to clouds is required to make decisions on whether the site is available to close a link based on the available link margin. Generally, communication through thin clouds (attenuation less than 3 dB) may be possible, but the quality of the signal may vary significantly over short periods of time and will depend on the link margin allocated for clouds. For example, the sky may be partially obscured with thin cirrus clouds that are producing average transmission losses within the available link margin (e.g., three dB). However, small areas of more opaque cloud where transmission losses would exceed the available link margin may exist within the larger cirrus cloud layer. Cloud attenuation should

be measured at time scales on the order of a minute to a few minutes to identify and characterize such conditions.

5.3.1.4 Aerosol Attenuation, Sky Radiance, and Particle Distribution

In general, the atmospheric attenuation due to aerosols and sky radiance and the particle distribution do not vary significantly on minute timescales. The atmosphere is much more homogeneous with respect to aerosols than clouds. Therefore it is anticipated that it will be sufficient to collect measurements of aerosols and sky radiance at a time scale of once per 10 minutes.

5.3.1.5 Standard Meteorological Quantities

The standard surface meteorological variables of temperature, wind, relative humidity, and pressure are important to collect on time scales of minutes to an hour. Issues of condensation are an important consideration when making decisions on dome closures to protect the sophisticated optics inside. In addition, each ground station will have a wind speed threshold above which the dome can no longer be safely kept open for optical communications. Given the high variability of winds and risk of high winds in some conditions, it may be desirable to measure wind speed more frequently than temperature and relative humidity and pressure, probably on the order of minutes instead of once per hour.

5.3.2 SECONDS TO MINUTES

5.3.2.1 Optical Turbulence (Atmospheric Seeing Parameters)

As discussed in 2.2.3, OT can produce a significant degradation to the optical communications link. OT also varies much more rapidly than do clouds, with significant changes occurring on time scales of milliseconds to seconds. Although decisions on handovers may not be made based on OT, it is important to use this data to describe any link outages or fading in the absence of clouds. In addition, OT may influence decisions on data rate adaptations; that is, it may adjust data rates to recover link margin lost because of an increase in OT. While it may be important to characterize OT on millisecond time scales for atmospheric science applications, for any operational or statistical considerations in optical space communications it is largely sufficient to collect the relevant OT parameters (Fried coherence length [r_0], scintillation, and isoplanatic angle) on timescales of several seconds to a minute (see reference [36]).

6 USING THE PHYSICAL QUANTITIES FOR LONG-TERM CHARACTERIZATION AND REAL-TIME DECISION MAKING

6.1 LONG-TERM CHARACTERIZATION

6.1.1 GENERAL

The long-term characterization of clouds, optical turbulence, aerosols, and standard meteorological quantities is very important to the design of optical communications systems. The data can be used for many purposes including the physical design of the ground station, the design of AO systems, development of link handover strategies, and estimation of long-term system performance. The use of long-term data is discussed in the following subsections as it pertains to mitigating the effects of the atmosphere.

6.1.2 CLOUDS

The effective mitigation of communication outages due to clouds is improved by knowing the long-term cloud statistics. Reliable groundwork for cloud mitigation strategies has already been established, and has been used in support of NASA investigations of both deep space and near-Earth optical communications (see references [1], [37], and [61]). Two capabilities have proved invaluable in support of these studies: (1) the ability to obtain a long-duration, high-fidelity, and highly accurate cloud climatology (see references [63], [64], and [68], and (2) an optimization tool that seeks to find networks of sites that provide high CFLOS availability for a chosen CONOPS.

Over the last two decades, the United States (US) Government has developed a sophisticated, high fidelity cloud database customized for optical communication applications. The cloud climatology is derived from data provided by visible and infrared sensors aboard geostationary meteorological satellites including the US National Oceanic and Atmospheric Administration (NOAA) Geostationary Operational Environmental Satellite (GOES) program (see reference [38]), the European Meteosat Second Generation (MSG) program (see reference [39]), and the Japanese Multifunctional Transport Satellite (MTSAT) program (see reference [40]).

The Cloud Mask Generator (CMG) (see reference [37]) ingests the raw infrared and visible radiance images from these satellites. Using clear-sky background modeling and threshold tests, the CMG determines the probability for the existence of clouds in each pixel in the image. The horizontal resolution of the database is approximately 4 km and the temporal resolution ranges from 15 minutes over the Continental United States (CONUS) to hourly Outside of CONUS (OCONUS). Recently, a real-time 1-km version of the CMG was developed to support the Lunar Laser Communications Demonstration (LLCD).

Using CMG, cloud retrievals have been developed for a 29-year period (1995-2023) over CONUS and Hawaii for the purposes of long-term characterization of clouds specifically for optical communication applications. The CMG OCONUS database consists of 18 years (2005–2023) of hourly retrievals for the following regions: Chile and the Rio de Janeiro areas (South America), Ascension Island (Atlantic Ocean), Canary Islands, Spain and Italy, parts of

South Africa, parts of South Korea and Japan, and the Perth and Canberra areas in Australia. The CMG can also be used to develop new cloud analyses for regions in addition to those indicated above. This CMG cloud database has been validated against in-situ data during LLCD, but could benefit from a more extensive validation using long-term characterization of clouds derived from ground-based instruments at the OGS. More recently an artificial intelligence version of the CMG has been developed which requires far less computational time with improved quality (see reference [59]).

The selection of the optimal combination of sites cannot be determined by a simple analysis of the cloud statistics of individual sites. Rather, it requires an optimization algorithm that takes into account the correlations of multiple sites. This process may lead to the selection of one or more sites that have lower probabilities of CFLOS than sites not selected, but have cloud cover that is less correlated with other sites in the network.

The Laser communications Network Optimization Tool (LNOT) is an example of a program created to use the cloud databases developed by the CMG to compute the optimal configuration of sites based on a specific mission scenario (e.g., deep space to ground) and other constraints like minimum elevation angle from the ground to the spacecraft (see references [37] and [57]). For each time step, LNOT computes whether the ground terminal has geometric visibility to the space terminal via a direct elevation angle calculation. If the elevation angle to the satellite is greater than a specified threshold and the site is determined to be cloud-free, then that site is considered available for communications. LNOT has incorporated the following mission scenarios into its software: GEO, Medium Earth Orbit (MEO), LEO, L1, L2, lunar, and deep space. First- and second-order statistics are accumulated and saved for each LNOT simulation to study the specific behavior of the optimized networks. Diurnal, monthly, seasonal, and interannual variations in network performance are computed.

Along with output from the CMG, LNOT has been used over the last two decades to study different mission scenarios including that of NASA's recent LLCD mission, as well as the upcoming Laser Communications Relay Demonstration (LCRD). In addition, many simulations using LNOT were conducted during the Interagency Operations Advisory Group (IOAG) Optical Link Study Group (OLSG) activities (see references [2] and [3]), demonstrating a number of mission scenarios including LEO, L1, L2, and Planetary missions. For example, for the OLSG study, LNOT was used to determine the number and locations of ground sites needed to achieve certain performance metrics in a polar-orbiting LEO scenario. Since LEO satellites do not have simultaneous visibility to multiple, geographically diverse ground sites, a cloud mitigation strategy other than handovers is needed to transmit the required amount of data. The satellite must be able to store data until it has access to a cloud-free ground site. To conduct this study, LNOT was updated with the capability to simulate the impacts of onboard satellite storage. Onboard storage allows the satellite to buffer data during periods of time when no ground station is available for communication (e.g., because of clouds or geometric visibility limitations). The satellite can then transmit the data to an available site at a future time. In this mode, LNOT computes the PDT of a network of ground sites for the given orbit and CONOPS. In one study, LNOT determined that for a Geostationary-to-Ground scenario, a four-site network including Haleakala (Hawaii), Tenerife OGS (Canary Islands), Table Mountain Facility (California), and Hartebeesthoek (South Africa) could achieve a PDT of up to 99.6 percent (see reference [3]).

Long-term cloud data collected by satellites will continue to be available in the future to support similar studies. In addition, cloud data collected by ground-based instruments can be used to supplement or replace the satellite-derived cloud data for OGS. In particular, the high-resolution data from ground-based instruments can be used to characterize cloud coverage as a function of time of year and time of day, as well as the lengths of communication outages due to clouds and the time between such outages. This capability is particularly valuable as it characterizes those cloud processes that occur on spatial and temporal scales too small for geosynchronous satellites to observe regularly.

6.1.3 OPTICAL TURBULENCE

Since OT degrades free-space optical communications links, it is important to understand the severity of OT in order to mitigate its effects on the link. Long-term measurements of OT parameters at OGS can be used to develop mitigation strategies and techniques for each ground station. Optical turbulence at a particular site is influenced to some degree by larger-scale atmospheric processes, but it is often affected more by local-scale features unique to the area surrounding the site. For years, astronomers have conducted extensive campaigns to characterize the OT conditions at candidate observatory sites. The measurements are generally taken with custom-built instruments such as a DIMM. Such measurements are vital to understanding the very small-scale (less than a few meters) turbulence conditions at a particular site, but such a campaign takes at least a year to capture conditions during all seasons and times of day (see reference [41]).

As a precursor to use of in-situ measurements, numerical simulations of OT can be employed to provide an estimate of optical turbulence conditions at OGS. While they do not capture local conditions such as small terrain features and man-made structures, numerical simulations offer many advantages over direct measurements. Simulations can be used to provide a long-term distribution of OT in weeks or months, as opposed to years, for any location on Earth. In addition, they provide a three-dimensional description of C_n^2 over regions of interest. This capability is often useful in identifying phenomena that create severe OT such as elevated temperature inversions that cannot be measured with a DIMM (see reference [42]).

An example of OT simulation is the use of a model used to predict tropospheric weather: Numerical Weather Prediction (NWP). NWP models are routinely used by meteorologists to predict everyday weather; however, in this application the NWP model is modified to make simulations of C_n^2 (see references [43] and [58]). NWP models are initialized with atmospheric measurements taken around the globe. These measurements include temperature, pressure, moisture, and winds measured by sources that include surface weather stations, radiosondes (weather balloons), ships, aircraft, and satellites. The Weather Research & Forecasting (WRF) model developed jointly by the National Center for Atmospheric Research (NCAR) and NOAA is used to develop climatologies of OT. The model is based on the Navier-Stokes equations, which are solved numerically on a three-dimensional grid. The model simulates four basic atmospheric properties: wind, pressure, temperature, and atmospheric water vapor. OT variables are derived from these four parameters.

The WRF model has been used to develop climatologies of OT for several regions around the world including Albuquerque, New Mexico, the summits of Hawaii, and Tenerife OGS. Details of the formulation of the simulation can be found in reference [42]. Figure 6-1 shows the cumulative distributions of both WRF-derived and in-situ measurements of the hourly Fried Parameter (r_0) as a function of time of day at a site in Albuquerque, NM. The median and 5th and 95th percentile values of the distributions are shown. Data is referenced to a wavelength of 1550 nm and to zenith pointing. Results show a good correlation between the model and actual measurements. The Fried coherence length, r_0, varies significantly by time of day with large (benign) values of r_0 observed and modeled at night, and lower values observed and modeled during the warmest time of the day. The overall difference between r_0 values generated using the WRF model and observations is approximately 8 percent.

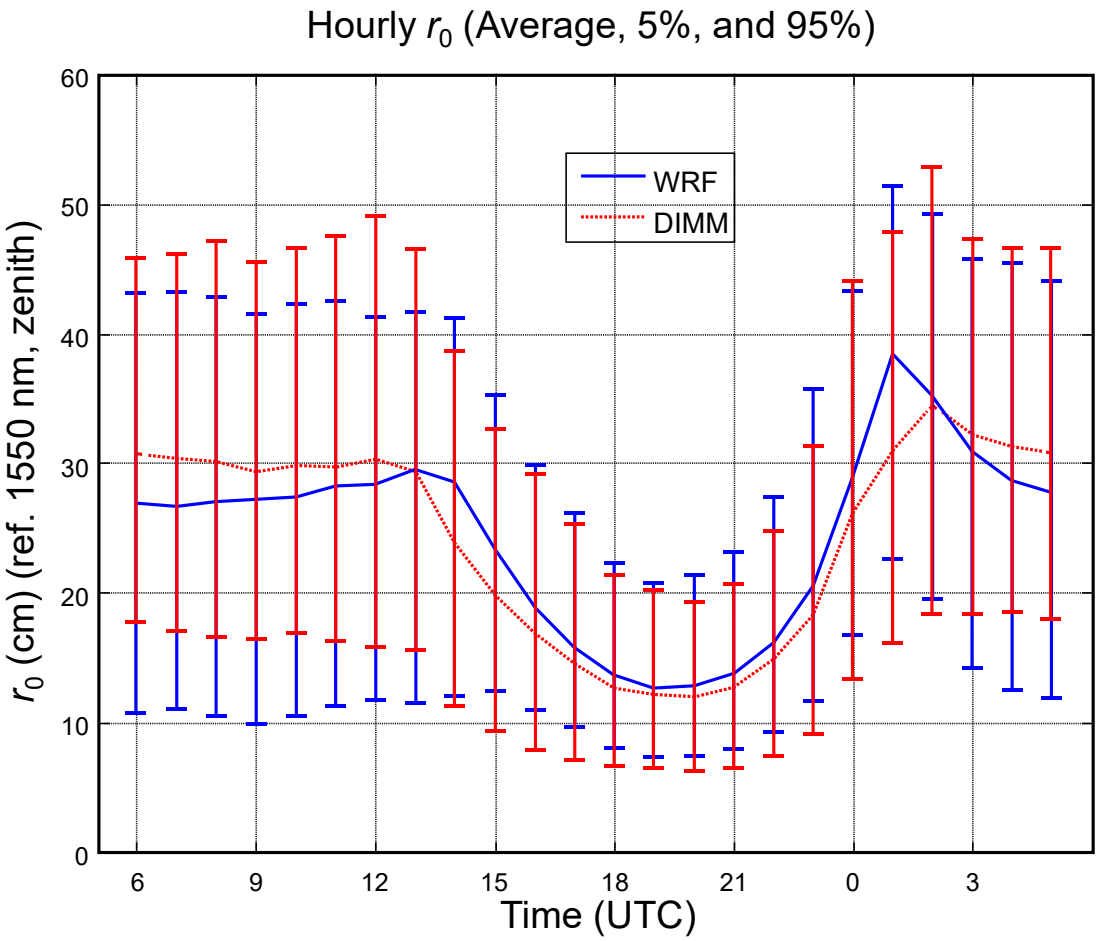

Figure 6-1: Hourly r_0 Derived from WRF and Compared to In-Situ Measurements at Albuquerque, NM

NOTE – In figure 6-1, data is referenced to 1550 nm and zenith. Comparisons are based on two years of simulations and DIMM measurements (see reference [42]).

6.1.4 AEROSOLS

Except under the most extreme conditions, attenuation of the optical communications link resulting from aerosols should generally be accounted for by available link margin. The link margin required for a particular CONOPS or a particular site can be determined by long-term measurement of attenuation due to aerosols in the atmosphere. Such measurements have been collected with Sun photometers at many locations on Earth for years by AERONET. A similar instrument deployed at OGS can be used to develop a distribution of aerosol attenuation that describes aerosol characteristics by time of year, time of day, and for a range of elevation angles. The measurements can also be used to identify the probability of occurrence of severe attenuation (e.g., more than 1 dB) due to aerosols at each location. This information can be used to modify the link budget or to develop mitigation strategies to account for such events.

6.1.5 STANDARD METEOROLOGICAL QUANTITIES

The equipment at each OGS should be designed to operate in the common weather conditions that occur at that site. Proper design should take into account the expected ranges of standard meteorological parameters: temperature, wind speed, relative humidity, and atmospheric pressure. Measurements should be taken at an OGS over a long period of time to capture the range of conditions. It is important to know how often condensation can be expected to form on the equipment so that any impacts can be mitigated. It is also important to build the physical structure to withstand severe weather conditions such as strong winds that occur at the OGS. It may be necessary to close a ground station under certain conditions to prevent damage to sensitive equipment or the physical structure. Long-term measurements of the standard meteorological quantities can be used by system designers to account for these situations in their design of the structures and operational concepts.

6.2 REAL-TIME DECISION MAKING

6.2.1 GENERAL

The ability to predict interruptions in the optical link resulting from the atmospheric effects is vital to the realization of highly available optical communications systems. Even at the best locations, the atmosphere will disrupt operations. Interruptions to the link are dominated by the presence of clouds. Clouds are the primary factor driving link-handover decisions, which ultimately impact the availability of the system. Therefore cloud predictions will drive the real-time decision making, and utilization of a strategy to minimize cloud interruptions will improve system performance. The design of the strategy will be dependent upon the CONOPS of a particular system and should consider such things as the number of terminals on the spacecraft, the number of ground stations visible to the spacecraft, the time required to repoint the terminal from the current ground station, and the time required to acquire the signal at a new ground station. For example, for a CONOPS with one satellite and two ground stations, A and B, station handover may be accomplished with either a ‘make before break’ or a ‘break before make’ methodology. In a ‘make before break’ CONOPS, there is more than one communications terminal on the satellite, and a link with a new site can be

established before the current link is broken. For a 'break before make' CONOPS, there is assumed to be only one terminal on the satellite, and communications must end with one site before a link can be established with a different site.

Standard meteorological quantities such as wind can require dome closures and therefore are important to predict. Optical turbulence can have an impact on the quality of signal, and is expected to be used only as a diagnostic for explaining link performance. Aerosols generally do not require prediction since their impact will be accounted for in the link budget. However, for dome closure decisions foreknowledge of impending dust storms would be desirable. Therefore these factors are only briefly discussed in the following subsections.

6.2.2 TIME SCALES FOR ATMOSPHERIC PREDICTIONS

6.2.2.1 General

Predictions of future weather conditions can be made on various time scales, from seconds, to minutes, to several days (see reference [60]). The amount of time between the current time and the time at which some event or action is to occur is referred to as the 'lead time'. For example, if the ground-based cloud instrument predicts a cloud will interrupt a currently active optical link in five minutes, the forecast lead time is five minutes, and a decision must be made to either accept the outage or repoint the space terminal to an alternate site that is projected to be cloud-free in five minutes. The relevant ground stations must also be determined beforehand and be ready to acquire the spacecraft on correspondingly short notice. The amount of lead time required for weather predictions will vary with the system CONOPS, and will be a function of the distance between the space terminal and the ground. For example, communications from deep space involve a longer lead time than near-Earth communications. Recommendations are made as to the forecast lead time for each case.

6.2.2.2 Minutes

A predictive weather system for free-space optical communications should be able to assess whether the current conditions are favorable for communications in the network at all sites that have visibility to the space terminal. It should be able to predict how long those conditions will continue, that is, when the next interruption will occur. The system should also be able to identify poor conditions and predict when conditions will improve. Although highly dependent on the CONOPS of any given system, for near-Earth applications it is recommended that weather predictions, and clouds in particular, have a lead time of several minutes.

6.2.2.3 Hours

A deep-space-to-ground scenario may require an hour or more of lead time to predict CFLOS and other weather conditions because of the long transit time. For example, in a Mars scenario the transit time may approach 30 minutes and require at least an hour lead time for the CFLOS prediction. Geostationary and LEO CONOPS may also require hour-long predictions for scheduling and handovers.

6.2.2.4 Days

Weather predictions a day or more in advance may be required to support the scheduling of sites supporting multiple missions. Optical space communications, in particular, often require an interagency cross-support scenario where stations support multiple satellites. Furthermore, lead times of one or more days can enable effective scheduling of station maintenance, which is often best executed during times when sites are predicted to be unavailable because of poor weather conditions. Uncertainty associated with longer-range forecasts beyond a day will have to be factored in to the scheduling process.

6.2.3 TOOLS AND METHODS FOR ATMOSPHERIC PREDICTIONS

6.2.3.1 Overview

Future atmospheric conditions can be predicted in a variety of ways. Some are better suited to short-term predictions, while others provide longer-term forecasts. Although dependent on system CONOPS, most atmospheric prediction strategies should combine short-, mid-, and long-range forecast leads times. The following subsections discuss three different possible forecast methods that could be deployed based on specific requirements. Other approaches not described in this Report may also be suitable.

6.2.3.2 Persistence

The persistence forecast predicts that whatever is observed at the current time will persist for some time into the future. For example, if the whole sky imager indicates a CFLOS at the current time, then the persistence forecast says that a CFLOS will be maintained indefinitely. By definition, the persistence forecast does not predict a change of state. Ultimately the persistence forecast will fail because the current CFLOS state will not last forever. A persistence cloud forecast is most helpful for very short-range forecasts on the order of a few minutes to maybe as much as one half hour. For some FSOC applications this type of forecast may be all that is necessary to maintain high link availability. Figure 6-2 shows the probability that, given a site is cloud-free, it will remain cloud free for some specified time. The probabilities are derived from GOES-derived cloud analyses over the period 1997–2013 at 15-minute resolution. The probability of a conditional clear period lasting one hour or longer diminishes to 55 percent–65 percent and further drops to 35 percent–45 percent by three hours. This finding shows that errors using a persistence forecast grow rapidly with time. Although these results were obtained from satellite-based cloud data, the principle is the same for a ground-based cloud sensor. The advantage of the ground-based cloud sensor (e.g., WSI) is that the data is available more frequently and at higher spatial resolution, allowing more accurate persistence forecasts at time scales of seconds to minutes.

Persistence forecasting can be used for any atmospheric parameter, and should be a consideration for short-term predictions out to a few minutes.

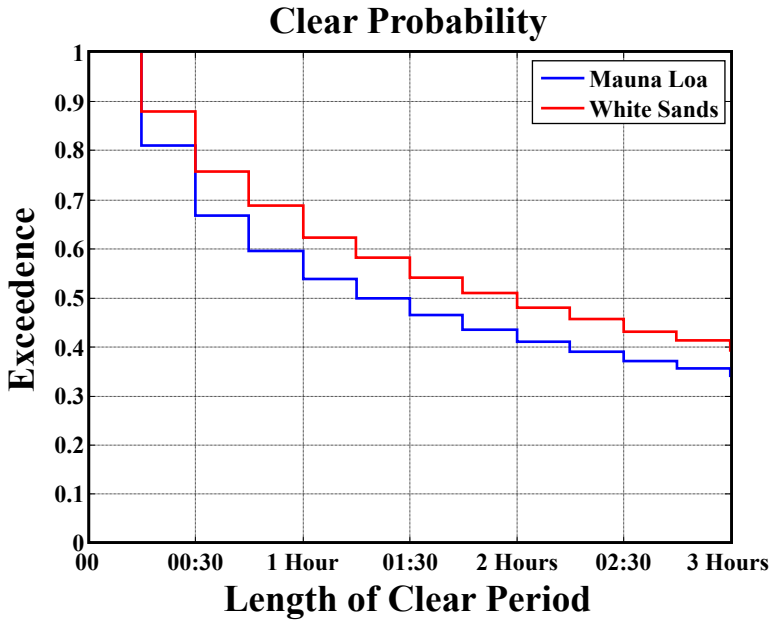

Figure 6-2: Conditional Probability of Cloud-Free Duration for Sites at Mauna Loa and White Sands

6.2.3.3 Advection (Recent Cloud Motion)

A cloud forecast can be derived from the recent motion of cloud elements, whether they be observed from a satellite looking down or from the ground looking up. The idea behind the advection forecast is to look for patterns in motion and assume they will continue over some period of time. An example of an advection cloud forecast is the Cloud Propagator Forecast (CPF) (see reference [44]). The CPF operates on successive cloud analyses to produce reliable probability forecasts of future cloud cover conditions at each point location. Alternatively, the CPF can forecast the expected amount of sky cover in a local sky dome about each point location. The CPF uses the CMG dataset as an input and produces a forecast valid at a specified time in the future. The CPF retains model data from previous runs for the same location, and is capable of boot-strapping itself rapidly if no prior-run model data are available.

Results have shown that the cloud advection forecast may be superior in skill to the simple persistence forecast because it can predict change. It is intended to be a short-term forecast for lead times of a few minutes out to one or two hours, and will work well for organized, well-behaved cloud systems with consistent movement in a single direction. However, the advection forecast will not generally perform well in situations where clouds are forming and dissipating on short time scales on the order of minutes. Figure 6-3 shows the correlation between CPF forecasts and truth at White Sands, NM. A forecast lead time of two hours is generated. The correlation between forecast and truth starts at 1.0 for the zero hour forecast and decreases to approximately 0.9 by two hours. The correlation is for both cloudy and clear forecasts.

Applying an advection scheme such as the one described above on in-situ data from a WSI would also be an attractive way to produce short-term cloud forecasts for handover decisions, although much work would be required to mature the technique. The CPF represents but one type of cloud advection type algorithm. Other algorithms could make use of neural networks that train the algorithm based on many types of situations.

There is no analogous advection method for meteorological parameters such as temperature and wind speed.

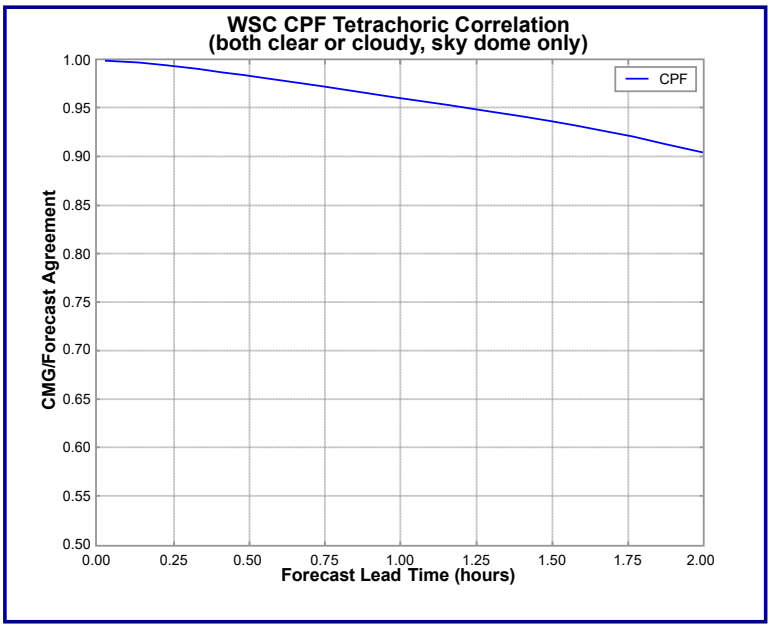

Figure 6-3: Tetrachoric Correlation between CPF and Truth at White Sands, NM

6.2.3.4 Numerical Weather Prediction

There may be some FSOC applications that could benefit from longer-lead cloud predictions. For example, the ability to predict whether a site will be cloudy so that maintenance can be scheduled may be desirable. Predictions of the time and length of an upcoming network outage could also benefit data dissemination strategies. The simple persistence and advection techniques may be beneficial for periods as long as several hours. However, they have no ability to predict the formation and dissipation of clouds.

NWP uses mathematical models of the atmosphere and oceans to predict the weather based on current weather conditions. A number of global and regional forecast models are run worldwide using current weather observations relayed from radiosondes (i.e., weather balloons) or meteorological satellites as inputs. Factors affecting the accuracy of numerical predictions include the density and quality of observations used as input to the forecasts, along with deficiencies in the numerical models themselves. Generally, there is skill in NWP forecasting out to five to seven days (see reference [62]).

Over the last decade, ensemble NWP forecasts have been used operationally to account for the stochastic nature of weather processes—that is, to resolve their inherent uncertainty. The ensemble method involves analyzing multiple forecasts created with an individual forecast model by using different physical parameterizations or varying initial conditions. The goal is to better define the uncertainty in the forecast. The ensemble method may be an important capability for predicting clouds and weather conditions for FSOC applications. Although the NWP models lack the horizontal resolution necessary to completely describe the line-of-sight from the ground to the communications satellite, they can provide horizontal resolution as high as 1 km. Typically, however, NWP models provide horizontal resolutions that describe cloud systems on scales of 10 km.

As an example of the accuracy of NWP cloud forecasts, a result from a study conducted in support of the NASA LLCD project in 2013 is shown in figure 6-4. The data in the figure show the correlation between two different ensemble NWP systems and the actual satellite-derived cloud coverage for White Sands, NM, over an 11 month period. The forecast lead time ranges from 84 hours for the Short Range Ensemble Forecast (SREF) to nearly 120 hours for the Global Ensemble Forecast System (GEFS). The SREF system is a regional model (CONUS only) composed of 21 independent models or members that predict many parameters, including the cloud fraction at all grid points in its domain (see reference [45]). The horizontal resolution of the SREF model is approximately 12 km. Its correlation with the actual cloud fraction measured by the GOES satellites ranges from 0.8 at 6 hours to 0.6 at 84 hours. The GEFS system is also composed of 21 members, but it is a global model, meaning it provides forecasts for the entire Earth. Because of its larger domain size, GEFS is run at a coarser horizontal resolution (1 degree) than the SREF to ensure its completion within a reasonable amount of time. The GEFS correlation with the satellite-derived cloud coverage is somewhat worse than the SREF, with a correlation coefficient of about 0.7 for a 6-hour forecast and 0.5 at 120 hours (5 days). This result is most likely due to the coarser resolution of the GEFS, and its inability to resolve cloud features at scales on the order of tens of kilometers.

NWP models are run daily by multiple weather agencies all over the world to develop weather forecasts that are used to protect life and property. Furthermore, they are the focus of many validation studies and undergo research and development on a regular basis. Although the cloud forecasts are not nearly perfect at the current time, further improvements to NWP technology will undoubtedly increase the cloud forecast reliability at forecast lead times of a few hours out to a few days. One area of improvement would be to assimilate local cloud information from WSI into the model, which would improve initial conditions and produce a better-quality forecast.

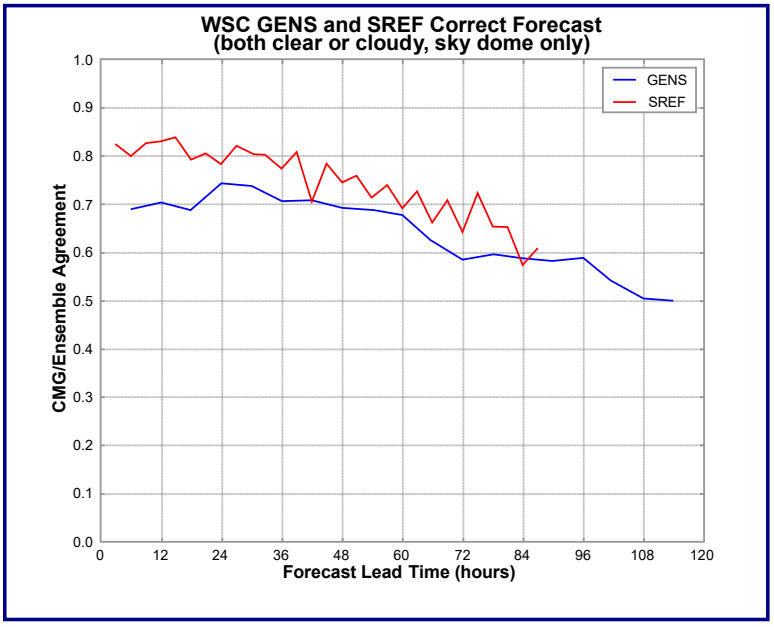

Figure 6-4: The Probability of Agreement between Ensemble NWP and Truth

In addition to cloud coverage, NWP models can also be used to provide predictions of the standard atmospheric parameters of temperature, wind, relative humidity, and pressure. These are standard model outputs, and may be useful to prepare for ground station closures due to unusual or damaging weather conditions.

ANNEX A

ADDITIONAL PHYSICAL QUANTITIES

A1 INTRODUCTION

Additional factors such as Rayleigh scattering, molecular absorption scintillation, the particle distribution, and surface contamination can be used for general characterization of the optical channel at a given site. The real-time values of these additional physical quantities are not critical for the site selection or system operation. Each of these quantities is detailed below.

A2 RAYLEIGH SCATTERING

A number of analytical models are available to characterize the impact of Rayleigh scattering on the optical depth with high fidelity (see reference [46]).

Rayleigh or molecular scattering is caused by the interaction of bound electrons of molecules or atoms of gasses in the atmosphere with the incident light. The magnitude of Rayleigh scattering mainly depends on the gas concentration as it relates to the observation locations (see reference [46]). One can approximate the Rayleigh optical depth to first order as:

$$\tau_m^s\left(\lambda_i\right) = \frac{p}{p_o} 0.00877 \lambda_i^{-4.05}, \tag{15}$$

where p is the atmospheric pressure at the location of interest, p_o is the atmospheric pressure at sea level, and the wavelength λ_i is in microns. The exponent term in equation (15) clearly indicates that at longer wavelengths the effects of Rayleigh scattering are greatly reduced, resulting in a smaller contribution of molecular scattering in the total atmospheric transmittance.

Radiative transfer codes, such as MODTRAN and Fast Atmospheric Signature Code (FASCODE) can also calculate values of Rayleigh optical depth for locations of interest when appropriate atmospheric conditions are input into the model (see reference [47]). As an example, figure A-1 provides a visual description of the total atmospheric transmittance (blue curve) plotted against the portion of atmospheric transmittance related/caused by Rayleigh scattering (black curve). These data were produced using MODTRAN code simulation data, and describe a vertical path at sea level in the wavelength range 320-1700 nm. The effects of Rayleigh scattering are scarcely detectable at wavelengths larger than 1000 nm, and while the scattering increasingly affects the atmospheric transmittance in the visible, it is even greater in the UV range.

The Consultative Committee for Space Data Systems

Report Concerning Space Data System Standards

REAL-TIME WEATHER AND ATMOSPHERIC CHARACTERIZATION DATA

INFORMATIONAL REPORT

CCSDS 140.1-G-2

GREEN BOOK

March 2024

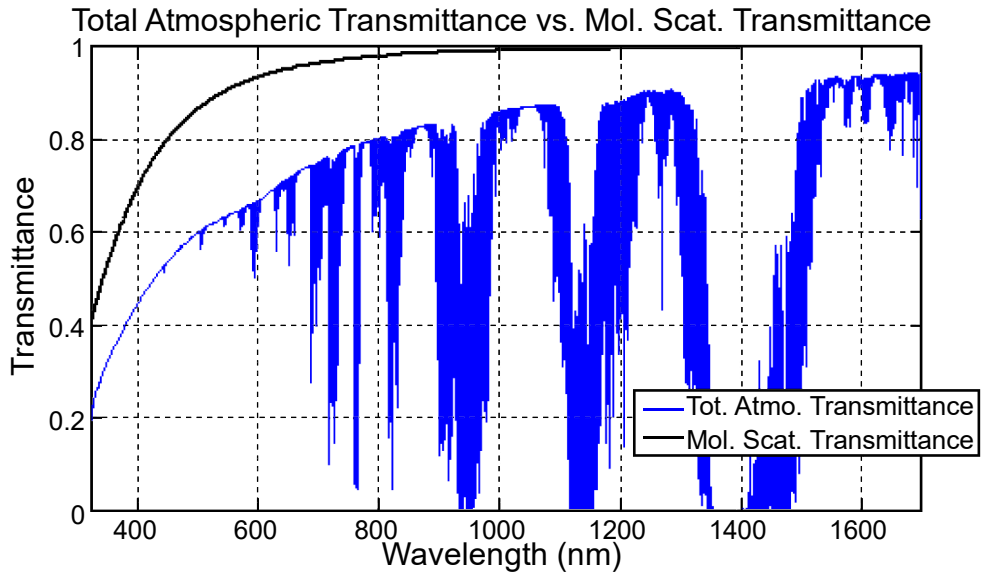

Figure A-1: Example of Spectrum of Total Atmospheric Transmittance and Molecular (Rayleigh) Scattering Transmittance

NOTE – In figure A-1, the curves describe a ground-to-space scenario at zenith. The example is for ground at sea level with clear sky and rural aerosol distribution. The curves are obtained after of the atmospheric modeling using MODTRAN, a radiative transfer code.

A3 MOLECULAR ABSORPTION

Molecular absorption occurs when the photon energy of the propagating beam is absorbed by the molecules or atoms of the gasses composing Earth's atmosphere. Molecular absorption manifests itself with very narrow absorption lines (sub-angstrom) in the atmospheric transmittance spectrum, reducing the transmittance within the absorption line close to zero. As an example, the impact of molecular absorption on the total transmittance spectrum (blue curve) is shown in figure A-1 by the deep absorption lines.

A number of radiative transfer codes are currently available to calculate the effects of molecular absorption under different atmospheric conditions. A software application regularly used to calculate molecular absorption is FASCODE (see reference [48]).

FASCODE can cover a wavelength range from the UV to the infrared, and describes absorption lines with a resolution of up to 0.001 cm^{-1}. In FASCODE, characteristics of atmospheric molecular components with their related (over one million) spectral absorption lines are described in the HIgh-resolution TRANsmission (HITRAN) database (see reference [49]). FASCODE's reliability has been validated by a number of programs and studies (see reference [50]) and it is currently considered the benchmark for line-by-line atmospheric transfer codes.

A4 SCINTILLATION

A4.1 GENERAL

Because of optical turbulence, the distorted wavefront of the laser beam propagating in the atmosphere causes constructive and destructive interference within the laser beam's cross-section. The result is spatial and temporal fluctuation of the beam irradiance, which is called intensity scintillation. The main parameter for characterization is the intensity scintillation index, σ_I^2, a dimensionless parameter that describes the strength of the fluctuations of the laser beam. The scintillation index is the normalized variance of the beam intensity, and is defined by:

$$\sigma_I^2 = \frac{\left\langle I^2 - \langle I \rangle^2 \right\rangle}{\langle I \rangle^2}, \tag{16}$$

with I [W/m^2] being the intensity at the plane of observation.

For a downlink scenario, it is assumed that the electromagnetic wave is accurately modeled by a plane wave. In this case, the scintillation index, assuming a Kolmogorov turbulence spectrum of the optical turbulence, is given by (see reference [16]):

$$\sigma_I^2 = \exp\left[\frac{0.49\sigma_R^2}{(1+1.11\sigma_R^{12/5})^{7/6}} + \frac{0.51\sigma_R^2}{(1+0.69\sigma_R^{12/5})^{5/6}}\right] - 1, \tag{17}$$

where σ_R^2—a dimensionless parameter—is the Rytov variance that is related to the strength of the optical turbulence by (see reference [16]):

$$\sigma_R^2 = 2.25k^{7/6}\sec^{11/6}(\zeta)\int_{h_0}^{H} C_n^2(h)(h-h_0)^{5/6}dz\,. \tag{18}$$

Equation (18) describes the Rytov variance as a weighted path integral of the optical turbulence structure index coefficient C_n^2 [m$^{-2/3}$], indicating that the main contribution to σ_R^2 is caused by turbulence layers far away from the receiver. In equation (18), the height of the ground station is given by h_0 [m] and k [m^{-1}] is the wave number, while H is the height of the turbulence. The varying path section of turbulence is modelled by the power law of the secant of the zenith angle ξ [deg].

The scintillation index equals the Rytov variance σ_R^2 in the weak fluctuation regime when $\sigma_I^2 \approx \sigma_R^2 < 1$. Generally, a regime of moderate fluctuations is associated with $\sigma_R^2 \approx 1$ and a regime of strong fluctuations is associated with $\sigma_R^2 > 1$. The coincidence and deviation of the Rytov variance with/from the scintillation index for weak and strong fluctuations is clearly seen in figure A-2 (left). The graph shows the Rytov variance and scintillation index for two different C_n^2 profiles representing possible day and night conditions. In the figure, the Hufnagel-Valley profile (see reference [16]) is used to model the C_n^2 profile with ground

values of 1.7e-13 $m^{-2/3}$ (day) and 1.7e-14 $m^{-2/3}$ (night). Similarity between σ_R^2 and σ_I^2 can be observed until $\sigma_R^2 \approx 0.5$, which indicates the transition from weak to strong fluctuations.

The different regimes of scintillation index demand different statistical descriptions of the fluctuations of the signal irradiance. The Probability Density Function (PDF) of the signal irradiance due to scintillation is depicted in the right graph of figure A-2. Skewness to lower power levels increases with increasing scintillation index. In a weak fluctuation regime, a lognormal shape accurately describes the PDF. At larger Rytov variance values, the signal statistics turn into a gamma-gamma distribution (see reference [16]).

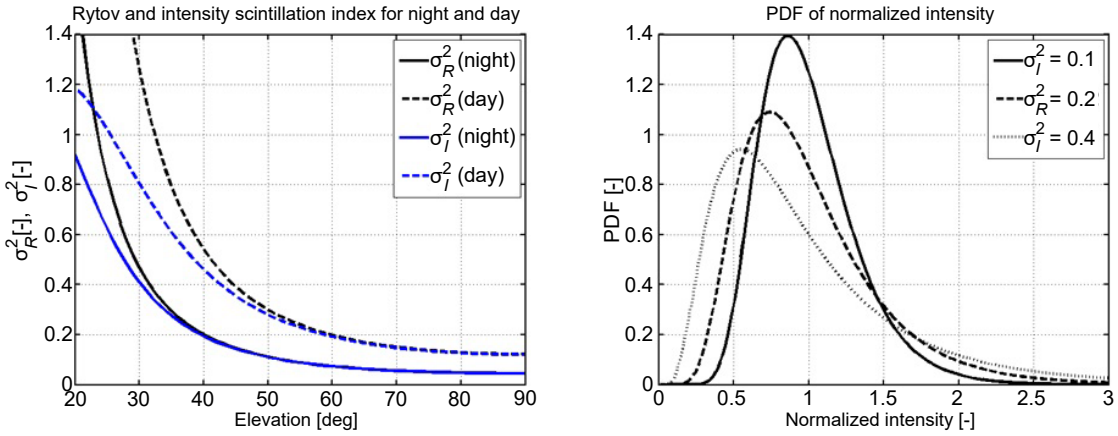

Figure A-2: Rytov Variance and Scintillation Index over Elevation for Examples of Nighttime (C_n^2=1.7e-14) and Daytime (C_n^2=1.7e-13) Conditions

NOTE – In the example in figure A-2, the ground station is placed at sea level, the wavelength is 1550 nm. The graph on the right shows PDF of normalized intensity for selected values of σ_I^2.

Scintillation effects on signal fading primarily affect the quality of an optical communication link by degrading the link Bit Error Rate (BER). If signal statistics and the fading temporal spectrum are known, the effects of signal fading on the BER can be ameliorated by designing appropriate channel coding and corresponding interleaving and/or retransmission schemes. Additionally, mitigation of scintillation is provided by the averaging effect of the ground station aperture (see reference [51]). For uplink applications that employ intensity modulation schemes (e.g., on-off keying), the use of multiple transmitter beams (transmitter diversity) can reduce the scintillation index of the signal at the flight terminal (see reference [52]).

A4.2 SCINTILLOMETER

Measuring signal fading due to optical turbulence can provide statistical characterization of the scintillation index of a particular site of interest. A typical measurement setup is shown in figure A-3, where a pupil camera is set up in the optical system to measure the signal beam intensity distribution in the pupil plane. The scintillation index is derived from the recorded

intensity images. In this configuration, care has to be taken that the signal intensity stays in the sensitivity range of the camera (i.e., no clipping, no underexposure). The scintillation index is derived from the processing of the images of the beam intensity at the pupil plane. Examples of measurements of scintillation index obtained with a pupil camera can be found in references [53], [54], and [55]. Care has to be taken that the signal intensity stays in the sensitivity range of the camera (no clipping, no underexposure).

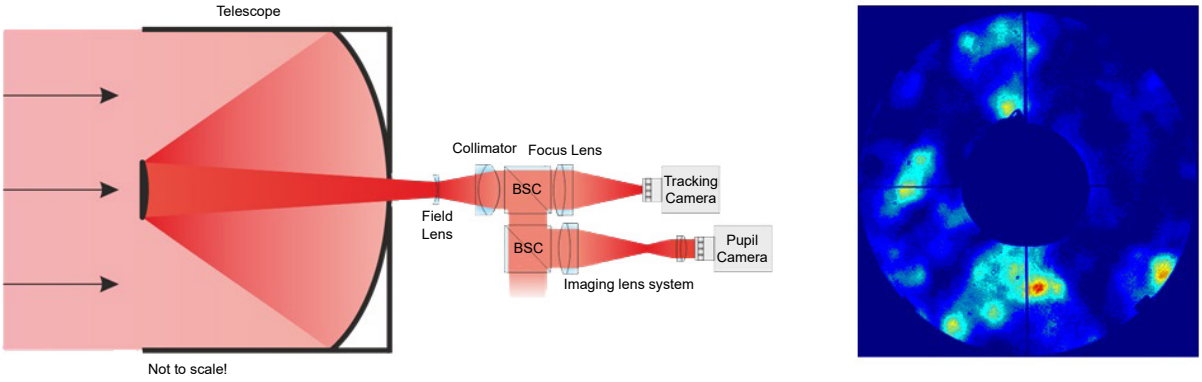

Figure A-3: Typical Measurement Setup

NOTE – In figure A-3, on the left is a block diagram of optical system for pupil camera measurements with tracking functionality. Aperture size here is 40 cm. On the right is an example snapshot of intensity in the pupil.

As a simpler alternative to a pupil camera, a photo diode can be installed in the focal plane for signal power monitoring. The advantage of this option is that the measurements can be taken at high sampling rates, enabling measurement of the temporal behavior of the scintillation. Measurement sources can be stars or satellites already in orbit. The sampling rate should be on the order of 10 kHz to adequately sample the whole fluctuation spectrum, including the case of a moving source (e.g., in LEO). However, the receiver telescope aperture must be kept small to guarantee that no aperture averaging takes place and only intensity statistics are measured. The aperture size should be smaller than the expected correlation width of intensity, which is typically on the order of several centimeters. The measurement setup in figure A-3 had spatial sampling of about 0.5 mm.

A5 PARTICLE DISTRIBUTION AND SURFACE CONTAMINATION

A5.1 GENERAL

Optical noise due to stray light originating from contamination can reduce the receiver SNR, which reduces the link performance, especially for low photon flux optical links. Therefore monitoring of the particle distribution and surface contamination is advised for low photon flux applications such as deep space scenarios.

The largest concentration of aerosols is in the boundary layer of the atmosphere. Particles suspended in air may deposit on the surface of mirrors of receiver ground stations, changing their optical qualities. An example of this process is the scattering of the Sun irradiance (stray light) caused by the particles deposited on the telescope primary mirror (see reference [56]). The particle distribution is measured via a particle profiler (see A5.2).

The level of stray light due to contamination is described with the help of the Bidirectional Reflection Distribution Function (BRDF). The BRDF is larger at higher contamination levels (higher particle deposition levels) and at smaller separation angles between the Sun and the ground station direction of observation (see reference [56]). The spectral radiance, $SL_\lambda(\lambda_i)$, originated by the BRDF, can be computed as:

$$SL_\lambda(\lambda_i) = I_S(\lambda_i) BRDF\ T(\lambda_i)^m, \tag{19}$$

where $I_s(\lambda_i)$ is the Sun's spectral irradiance at the top of the atmosphere, $T(\lambda_i)$ is atmospheric transmittance, and m is the atmosphere air mass. The BRDF due to contamination can be directly measured using a scatterometer, or it can be (approximately) derived when the contamination level of the mirror is known (see reference [56]). After deriving the spectral radiance due to contamination, $SL_\lambda(\lambda_i)$, from equation (19), equation (20) determines the additional optical noise power captured by a receiver because of contamination of the (primary) mirror as:

$$P_{SL}(\lambda_i) = SL_\lambda(\lambda_i) A \Delta\lambda \Omega_s. \tag{20}$$

A5.2 PARTICLE PROFILER

Local measurements of particle sizes and concentrations close to ground can be provided by a particle profiler. Figure A-4 shows a particle profiler deployed at the NASA/JPL Goldstone facility. This instrument consists of an air pump that injects a constant air flux into an internal chamber, where a nephelometer is used to count particle concentration and size. A particle profiler provides particle counts over a discrete number of bin sizes. The specific instrument shown in figure A-4 measures particle concentration over eight bins that cover particle sizes ranging from 0.3 to 10 μm. The system update rate ranges from 1 to 60 seconds, which is adequate to cover the temporal variation of the outdoor particle concentration.

Figure A-4: Particle Profiler Deployed at the NASA/JPL Goldstone, CA Facility

NOTE – The instrument shown in figure A-4 measures aerosol particle concentration in the range 0.3-10 μm with a selectable update rate varying from 1 to 60 seconds.

ANNEX B

ABBREVIATIONS AND ACRONYMS

AERONET	Aerosol Robotic Network
AMOS	Advance Maui Optical and Space Surveillance
AO	adaptive optics
ASIVA	All Sky Infrared Visible Analyzer
ATST	Advance Technology Solar Telescope
BER	bit error rate
BRDF	bidirectional reflection distribution function
CCD	charge-coupled device
CCSDS	Consultative Committee on Space Data Systems
CDF	cumulative distribution function
CFLOS	cloud free line of sight
CMG	cloud mask generator
CONOPS	concept of operations
CONUS	Continental United States
COTS	commercial off-the-shelf
CPF	cloud propagator forecast
DIMM	differential image motion monitor
ESA	European Space Agency
FASCODE	Fast Atmospheric Signature Code
FOV	field of view
FSOC	free-space optical communications
FWHM	full width half maximum
GEFS	Global Ensemble Forecast System

GEO	geostationary
GOES	Geostationary Operational Environmental Satellite
HITRAN	high-resolution transmission
IOAG	Interagency Operations Advisory Group
IR	infrared
JPL	Jet Propulsion Laboratory
LCRD	Laser Communications Relay Demonstration
LEO	low Earth orbiting
LLCD	Lunar Laser Communications Demonstration
LNOT	Laser Communications Network Optimization Tool
LWC	liquid water content
LWIR	longwave infrared
MEO	medium Earth orbit
MODTRAN	Moderate Resolution Atmospheric Transmission
MSG	Meteosat Second Generation
MTSAT	Multifunctional Transport Satellite
NASA	National Aeronautics and Space Administration
NCAR	National Center for Atmospheric Research
NICT	National Institute of Information and Communications Technology (Japan)
NOAA	National Oceanic and Atmospheric Administration
NWP	numerical weather prediction
OCONUS	outside of CONUS
OGS	optical ground station
OGS-OP	Optical Ground Station Oberpfaffenhofen

OLSG	Optical Link Study Group
OT	optical turbulence
PDF	probability density function
PDT	percent data transferred
PSF	point spread function
RH	relative humidity
SDIMM	solar differential image motion monitor
SNR	signal-to-noise ratio
SREF	short range ensemble forecast
TMT	thirty meter telescope
UV	ultraviolet
US	United States
WRF	weather research and forecasting
WSI	Whole Sky Imager